UNIVERSIDADE DE LISBOA
FACULDADE DE CIÊNCIAS
DEPARTAMENTO DE ENGENHARIA GEOGRÁFICA, GEOFÍSICA E ENERGIA

Numerical analysis and experimental validation of pollutant dispersion for the actual urban area of Niigata city, Japan

Pedro Filipe Mendes Pereira

Mestrado Integrado em Engenharia da Energia e do Ambiente

2014

UNIVERSIDADE DE LISBOA
FACULDADE DE CIÊNCIAS
DEPARTAMENTO DE ENGENHARIA GEOGRÁFICA, GEOFÍSICA E ENERGIA

Numerical analysis and experimental validation of pollutant dispersion for the actual urban area of Niigata city, Japan

Pedro Filipe Mendes Pereira

Dissertação de Mestrado em Engenharia da Energia e do Ambiente

Trabalho realizado sob a supervisão de

Prof. Dr. Ir. Bert Blocken (TU/e)

Prof. Dr. Ir. Guilherme Carrilho da Graça (FCUL)

2014

Abstract

Computational Fluid Dynamics (CFD) is increasingly used to predict the wind flow and pollutant dispersion around buildings. One of the most frequently used turbulence used approaches in CFD is given by the Reynolds-averaged Navier-Stokes (RANS) equations.

In this research, prediction of pollutant dispersion around buildings was compared with wind-tunnel data for two model configurations: an isolated cubic building with a vent located on its rooftop (Case 1) and an actual urban area of Niigata city, Japan (Case 2). This analysis was made through both the wind flow and pollutant concentration field by using RANS.

For Case 1, three turbulence models were tested: the RNG k-ε model, the Realizable k-ε model and the RSM. Such models provided underpredicted results in relation to the wind-tunnel data from Li and Meroney (1983). Paying special attention to the recirculation on the rooftop, decreasing the turbulent kinetic energy (k) up to four times, results in a closer correspondence to the experiments. Only the Realizable k-ε model failed to reproduce significant recirculation of the wind flow on the rooftop. The RNG k-ε model and RSM presented fair results against measurements.

Case 2 presents a higher level of complexity than Case 1 because it treats an urban area which is characterized by irregular buildings and streets. Thus, it is more difficult to arrange a high-quality grid. A high-quality grid was created with a total number of cells higher than 60 million. One simulation was performed by using RANS. Results were validated using the wind-tunnel data provided by the Architectural Institute of Japan (AIJ). The wind flow field predictions showed good agreement. Concentration field predictions showed overpredicted results in some locations, however, in general, the results showed fair agreement with the wind-tunnel measurements.

Keywords : CFD; Pollutant dispersion; Buildings; Urban area; Turbulence modeling.

Resumo

A dinâmica de fluídos computacional (CFD) está em uso crescente no que respeita à previsão do fluxo de vento e da dispersão de poluentes ao redor de edifícios. Para modelar o fluxo turbulento as equações *Reynolds-averaged Navier-Stokes* (RANS) são frequentemente utilizadas em CFD.

Na presente pesquisa, a previsão da dispersão de poluentes é comparada através de valores obtidos em túnel de vento para duas configurações diferentes: um edifício isolado com um ventilador no topo deste (Case 1) e uma parte da área urbana da cidade de Niigata, Japão (Caso 2). Esta análise foi feita através do fluxo de vento e da concentração de poluentes usando RANS.

O Caso 1 usou três modelos de turbulência: modelo k-ε RNG, modelo k-ε *Realizble* e RSM. Todos apresentaram resultados subestimados em relação aos obtidos em túnel de vento por Li e Meroney (1983). Dando especial atenção à recirculação no topo do edifício, diminuindo o perfil da energia cinética de turbulência (k) até quatro vezes obtém-se resultados mais próximos das medições experimentais. Apenas o modelo k-ε *Realizable* falhou a previsão da recirculação no topo do edifício. Os modelos k-ε RNG e RSM apresentaram resultados aceitáveis perante as medições.

O Caso 2 apresenta uma complexidade superior ao Caso 1 porque trata uma área urbana caracterizada por edifícios e ruas irregulares. Assim, torna-se difícil criar uma malha de alta qualidade. Para o fazer, a malha apresenta um total de células superior a 60 milhões. Uma simulação foi conduzida usando RANS. Os resultados foram validados através da informação providenciada pelo Instituto de Arquitectura do Japão (AIJ). As previsões para o fluxo de vento mostram concordância. As previsões de concentração mostram valores sobrestimados em algumas localizações, mas em geral os resultados estão de acordo com as medições em túnel de vento.

Palavras-chave: CFD; Dispersão de poluentes; Edifícios; Área urbana; Modelação de turbulência.

Acknowledgment

Along eleven months I had the privilege of studying in the Eindhoven University of Technology (TU/e). I could work and learn on Computational Fluid Dynamics (CFD) with the best references in the field.

Dispersion modeling using CFD is growing. CFD is an useful tool for predicting the impact of pollutant sources in the urban environment, outside the buildings and which influence the pollutant dispersion has at the pedestrian-level. That prediction plays an important role on the re-ingestion of pollutants to inside the buildings and, consequently, on indoor air quality which directly affects human beings' health and productivity.

It was a pleasure to make part of the Building Physics and Services (BPS) department. I would like to express my gratitude to Professor Bert Blocken, Twan van Hooff and Wendy Janssen who daily supervised my work and gave me all kind of useful suggestions on this project.

I would like to thank to Professor Guilherme Carrilho da Graça who supported my work from my home institution, the Faculty of Sciences of the University of Lisbon (FCUL).

A special acknowledgment to Professor Yoshihide Tominaga who provided the data required for validating my results related with the urban area of Niigata, from the Architectural Institute of Japan and Niigata Institute of Technology.

I want to thank to my family and my fellow students for their support and motivation.

Thanks to João who shared with me this experience in Eindhoven and gave me important suggestions to this project.

Thanks to Laura for her important role in my life.

Pedro Mendes Pereira

Lisbon, October 2014

List of Figures

List of Tables

Content

1. Introduction

1.1 Air pollutant dispersion in the urban environment

Air pollution brings harmful particles to the atmosphere which strongly affects both health and productivity of the human beings. Different sources of pollutants contribute to the emission of those particles. Stacks and rooftop vents are examples of such sources which release pollutants on the atmosphere at the pedestrian-level. This pollutant dispersion is influenced by the wind flow and its direction, speed and turbulence, making possible reinjection of pollutants to inside the buildings through refrigeration openings and windows as demonstrated by the Figure 1.1.

Thus, pollutant concentration around buildings should be known to avoid harmful amounts of that concentration, mainly at the pedestrian-level (until 2 m high from the ground-level). For predicting pollutant dispersion is required to model the wind flow field. Knowledge about how buildings affect the wind flow field in the urban environment is a starting point on modeling it.

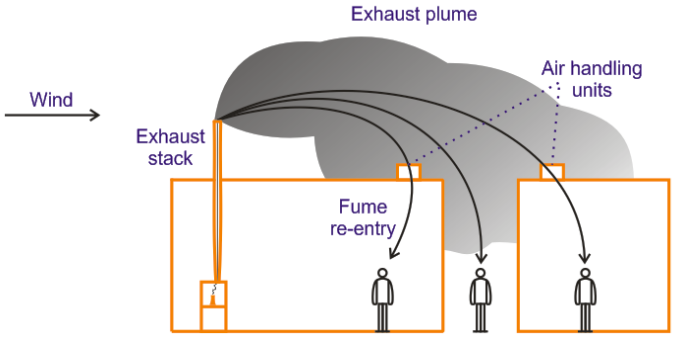

Figure 1.1 Diagram of air pollutant dispersion due reinjection of exhausted pollutants [1]

Obstacles, such as cubic buildings, influence the wind flow as shown in Figure 1.2-1.3 [2,3], through a two dimensional perspective, and in Figure 1.4, through a three dimensional one [4]. Figure 1.2-1.3 clearly show that exists separation of the wind flow in two parts in front of the building. A vortex and, consequently, recirculation of the wind flow occur in front, sides, top and behind the building (Figure 1.4) because of that separation.

That recirculation can cause backflow of pollutants released from rooftop vents and stacks bringing significant concentrations to the pedestrian-level and promoting their reinjection to inside the buildings. Thus, in order to limit this kind of phenomenon it is important to predict such concentration of pollutants and respective reinjection.

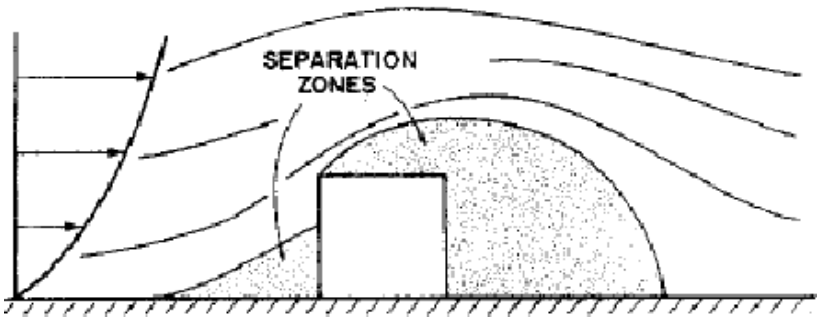

Figure 1.2 Two dimensional perspective of the wind flow separation near a cubic building [2]

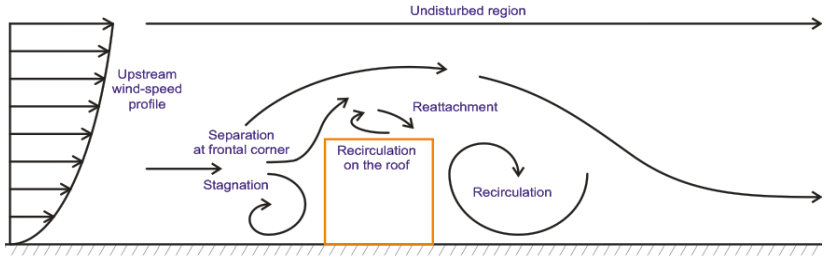

Figure 1.3 Two dimensional perspective of the wind flow motions around an isolated cubic building [3]

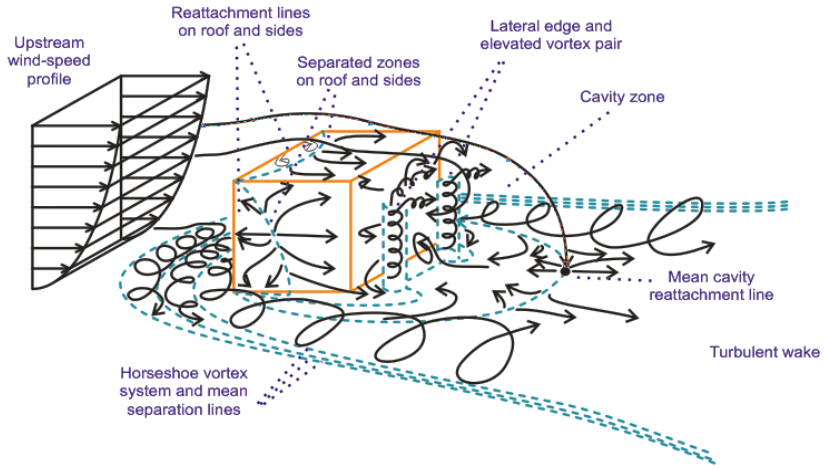

Figure 1.4 Three dimensional perspective of the wind flow motions around an isolated building [4]

1.2 Numerical modeling with Computational Fluid Dynamics

Computational Fluid Dynamics (CFD) is able to predict both the wind flow and pollutant concentration field through numerical simulation starting by modeling the atmosphere at the pedestrian-level. This encompasses definition of the equations for describing the wind flow and calculating parameters such as earth roughness and both the wind-speed and turbulence profiles at the inlet and outlet of the computational domain.

Reynolds-Averaged Navier Stokes (RANS), Large Eddy Simulation (LES) and Direct Numerical Simulation (DNS) are all turbulence model approaches for modeling the turbulent flow. RANS equations are the most used turbulence approach [1,5]. That approach requires application of models for modeling the turbulence. Those turbulence models available are the k-ε models, such as Standard, Realizable or RNG, and the Reynolds-stresses model (RSM). Based on literature, the most common turbulence models are the k-ε ones. All the turbulence k-ε models require a turbulent kinetic energy profile k and a turbulence dissipation rate profile ε as function of the computational domain's height. This is the meaning of k and ε.

CFD modeling requires validation of the results through comparison with wind-tunnel studies (reduced-scale experiments) or field measurements, also denominated full-scale experiments, for the same model configuration. It can be important to provide sensibility analysis of the grid arrangement, testing likely changes on the results with finer and coarser grids in respect to the number of cells. Parameters should be set precisely for limiting errors or deviations on the results. Such parameters are both the wind-speed and turbulence profiles at the inlet and outlet of the computational domain, earth roughness and conditions of the releasing sources.

1.3 Research objective

This project is being developed in the ambit of the final master thesis in Energy and Environmental Engineering. Briefly, the work consists on predicting the pollutant dispersion in the

urban environment by using numerical simulations in CFD, validating the predictions through wind-tunnel experiments. The work is split on two case studies that will be developed in the chapter 3 and 4. Finally, a global discussion, conclusions and final recommendations will be given in the chapter 5 and 6.

Case 1 aims to predict both the wind flow and pollutant concentration field which involves an isolated cubic building with a rooftop vent releasing pure helium (he). From west wind direction, several RANS turbulence models are tested such as it has been made by Gousseau et al. [6]. Predictions from Case 1 are then validated by comparisons against wind-tunnel experiments from Li and Meroney [7] whose model configuration and input conditions are the base of that numerical simulation.

Case 2 also aims to predict both the wind flow and pollutant concentration field but now involving an urban area of Niigata city, Japan. This urban area consists of a set of irregular buildings dispersed in the city through an irregular way along its perimeter. Those buildings present a height average of 6 m, but there are buildings from 2 m up to 60 m high. A pollutant source is set at the centre of the urban area, approximately. It is being released ethylene (C_2H_4) aiming to assess the pollutant dispersion taking into account wind direction and using RANS equations and the turbulence models available to be applied. Wind-tunnel experiments have been conducted by Tominaga et al. [8] for measuring the wind flow field and by the Architectural Institute of Japan (AIJ) [9,10] for predicting pollutant dispersion of ethylene. The AIJ provide results of both the wind flow and pollutant concentration field to validate the present research.

As a global goal, the present research aims to assess the potential of RANS and there turbulence models in predicting the pollutant concentration around buildings.

2. Literature study

2.1 Air pollutant dispersion assessment methods

The wind flow and pollutant concentration field can be predicted by experimental measurements, analytical methods or numerical modeling with CFD. Numerical modeling depends on such experimental setups for validation of case studies with similar model configurations. CFD can provide considerable amount of data information and modifications on the model can be easily tested. Its application is dependent on turbulence models which model both the wind flow and turbulence. Applying different turbulence models can conduct to discrepancies between the results for the same model configuration.

2.2 CFD modeling and methodology

In general, CFD procedure requires some choices such as the govern equations of the fluid flow, the sizing of the computational domain and its grid arrangement, which encompasses some parameters and boundary conditions that should be set: wind-speed and turbulence profiles at the inlet and outlet of the computational domain, earth roughness and the conditions in which a pollutant is being released from a source.

2.2.1 Governing equations

The following Navier-Stokes equations describe the fluid flow [3]:

$$\text{x: } \frac{\partial u}{\partial t} + \left\{u\frac{\partial u}{\partial x} + v\frac{\partial u}{\partial y} + w\frac{\partial u}{\partial z}\right\} = -\frac{1}{\rho}\frac{\partial p}{\partial x} + v\left(\frac{\partial^2 u}{\partial x^2} + \frac{\partial^2 u}{\partial y^2} + \frac{\partial^2 u}{\partial z^2}\right) + g \quad (1)$$

$$\text{y: } \frac{\partial v}{\partial t} + \left\{u\frac{\partial v}{\partial x} + v\frac{\partial v}{\partial y} + w\frac{\partial v}{\partial z}\right\} = -\frac{1}{\rho}\frac{\partial p}{\partial y} + v\left(\frac{\partial^2 v}{\partial x^2} + \frac{\partial^2 v}{\partial y^2} + \frac{\partial^2 v}{\partial z^2}\right) + g \quad (2)$$

$$\text{z: } \frac{\partial w}{\partial t} + \left\{u\frac{\partial w}{\partial x} + v\frac{\partial w}{\partial y} + w\frac{\partial w}{\partial z}\right\} = -\frac{1}{\rho}\frac{\partial p}{\partial z} + v\left(\frac{\partial^2 w}{\partial x^2} + \frac{\partial^2 w}{\partial y^2} + \frac{\partial^2 w}{\partial z^2}\right) + g \quad (3)$$

x, y, z: Cartesian co-ordinates;
u, v, w: velocities, m/s, along the Cartesian axes x, y, and z;
p: pressure, Pa;
ρ: density, kg/m^3;
g: gravitational acceleration, m/s^2.

Reynolds-Averaged Navier Stokes (RANS), Large Eddy Simulation (LES) and Direct Numerical Simulation (DNS) are all turbulence model approaches for modeling the turbulent flow. RANS equations are the most used turbulence approach [1,5]. That approach requires application of turbulence models once it only solves the mean wind flow. Those turbulence models are the k-ε models, such as the Standard, Realizable or RNG, and the Reynolds-stresses model (RSM). Based on literature, the most common turbulence models are the k-ε ones [5]. All the turbulence k-ε models require a turbulent kinetic energy profile k and a turbulence dissipation rate profile ε as function of the computational domain's height. This is the meaning of k and ε.

The turbulent Schmidt number (Sc_t) is associated to the turbulence k-ε models. It represents the ratio between the viscosity and diffusivity of turbulent flow and it can influence the simulation results [6]. Then, it is recommend to set it correctly when choosing the turbulence model.

2.2.2 Discretization

Before to start simulating, it is required some pre-processing. Pre-processing involves the sizing of the computational domain and its grid arrangement. For sizing the computational domain is imperative to establish ranges of distance from their boundaries to the reference obstacle creating a computational domain wide enough to avoid significant influence of it on the fluid flow around that reference obstacle. That reference obstacle, which can be a cubic building, has to be located five times its height far from the inlet, sides and top of the computational domain. In relation to the outlet, it has to be set ten times minimum far from that exit [11,12].

The spatial discretization of the computational domain should achieve a quality grid arrangement. The grid quality can be assessed through both the shape and size of the cells. All the cells should assume a close shape in relation to equilateral cells with the respective volume which is denominated skewness. Another attribute is related to the size of an adjacent cell and the following one. This is quantified by a ratio that states the length of a certain cell has to be 1.3 times maximum its adjacent cell length. It is denominated stretching ratio [13].

The grid arrangement can result in structured grids (Figure 2.1(a)), unstructured grids (Figure 2.1(b)) or hybrid ones (Figure 2.2) which means a combination of structured and unstructured parts in the same arrangement [5].

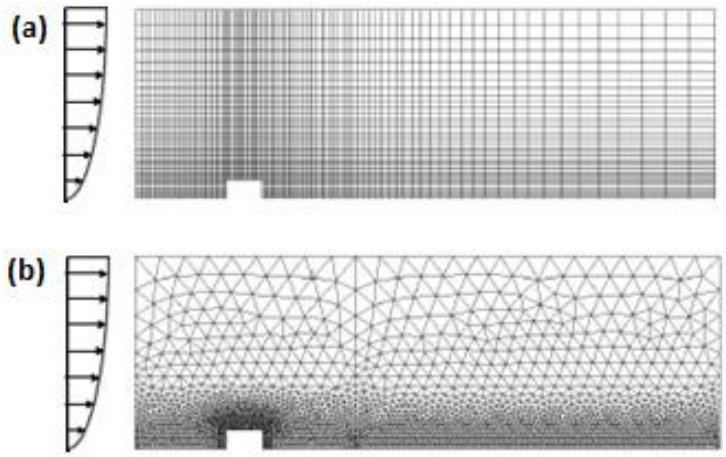

Figure 2.1 (a) Structured grid; (b) Unstructured grid (adapted from [5])

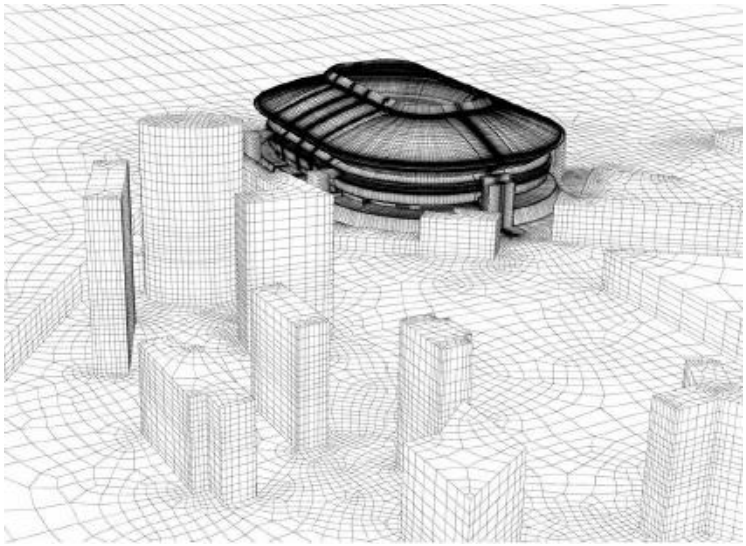

Figure 2.2 Example of a high-quality hybrid grid from van Hooff and Blocken [14]

After the discretization of the computational domain and before starting any simulation, it is required to set the govern equations, turbulence models, wind-speed and turbulence profiles at the inlet and outlet the domain, earth roughness and conditions of the releasing sources.

When the solution is achieved, post-processing is the next step by handling the data provided from the results. In CFD, it is possible to create figures by using colour scales which can define contours for the different levels of a variable such as the pollutant concentration. It makes that analysis more appellative and intuitive.

2.2.3 Boundary conditions

As previously described, before initializing any simulation, conditions should be set for characterizing the domain boundaries demonstrated in Figure 2.3. Those conditions are denominated boundary conditions [5].

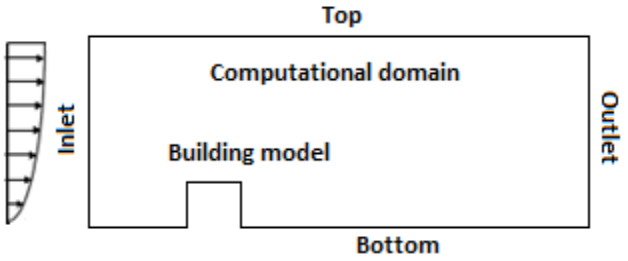

Figure 2.3 Computational domain and its boundaries: Inlet, Outlet, Bottom, Top and Building model (based on [5])

Generally, when conducting simulations by using RANS equations and turbulence k-ε models, profiles are defined for both the wind-speed (U) and turbulence, namely turbulent kinetic energy k and turbulence dissipation rate ε, at the inlet and outlet the domain. All those profiles are function of the domain's height and they can be obtained from the experimental setups used for validation whether provided by, or calculated based on the following equations (4)-(6) [15]:

$$U(z) = \frac{u^*}{\kappa} \ln\left(\frac{z+z_0}{z_0}\right) \quad (4)$$

$$k(z) = \frac{{u^*}^2}{\sqrt{C_\mu}} \quad (5)$$

$$\varepsilon(z) = \frac{{u^*}^3}{\kappa(z+z_0)} \quad (6)$$

$$u^* = \frac{\kappa U_{ref}}{\ln\left(\frac{z_{ref}+z_0}{z_0}\right)} \quad (7)$$

At the bottom, both the surface roughness z_0 and dimensionless roughness constant C_s have to be defined. Surface roughness is responsible for the mechanical turbulence increasing the wind-speed at the pedestrian-level in the lowest part of the atmosphere denominated atmospheric boundary layer (ABL). The surface roughness can be obtained from experimental setups of similar model configurations and it should be carefully set in order to keep a homogeneous ABL which is an imperative condition for the wind flow and turbulence profiles distribution.

Based on the grid arrangement, dimensionless roughness constant can be defined by fulfilling the following relationship between both the physical roughness height k_s and surface roughness z_0 [16]:

$$k_s = \frac{9.793 z_0}{C_s} \quad (8)$$

The physical roughness height k_s depends on the height of the grid first cell (y_0) that should be kept lower than 1 m at full-scale. It is stated that k_s should be set arbitrating a value lower than half y_0 (y_p) [16]. C_s is defined as a constant value when lower than 1 but, whether higher, it is provided by an user-defined function (UDF).

At the pollutant sources are set the vertical exhaust velocity of the pollutant released and the turbulence associated to the source's geometry. The exhaust velocity is defined from the wind-speed at the source's height (U_{ref}) multiplying it by the momentum ratio between such velocities. Momentum ratio is usually provided by the experimental setups. Also accordingly to the experimental setups is defined the turbulence intensity (I_u) and the turbulent length scale L_t which depends on the diameter of the source D_v for a circular one by using the following equation:

$$L_t = 0.07 D_v \quad (9)$$

Table 2.1 describes some parameters used in the previous equations.

Table 2.1 Equations parameters from (4)-(8) [15]

Parameter	Description
u*	friction velocity [m/s]
κ	von Karman constant ϵ [0.40;0.42]
z	domain height [m]
z_{ref}	reference height [m]
z_0	aerodynamic roughness length [m]
C_μ	turbulence model constant [-]
U_{ref}	mean wind velocity at reference height [m/s]

2.3 Pollutant dispersion studies

Experimental setups by using reduced-scale models and numerical studies with CFD will be presented. Some of these case studies will be used to validate results of the present research.

2.3.1 Reduced-scale experiments

Li and Meroney [7] created a reduced-scale model of an isolated cubic building with a rooftop vent releasing pure helium (he). Several wind directions and distinct vent positions on the rooftop have been tested aiming to measure the pollutant concentration field. Results focus the influence of those different wind directions and distinct vent positions on the rooftop recirculation of the wind flow (Figure 2.4) and recirculation behind the building. (Figure 2.5-2.6).

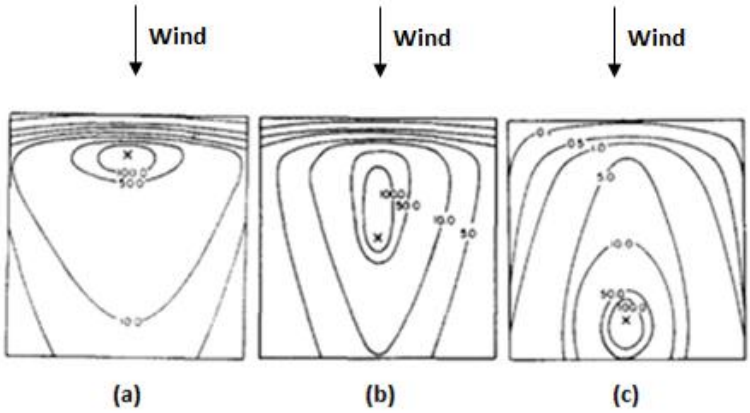

Figure 2.4 Pollutant concentration K on the rooftop for different rooftop vent locations represented as "x" (adapted from [7]): (a) located upwind; (b) located at the rooftop's centre; (c) located downwind

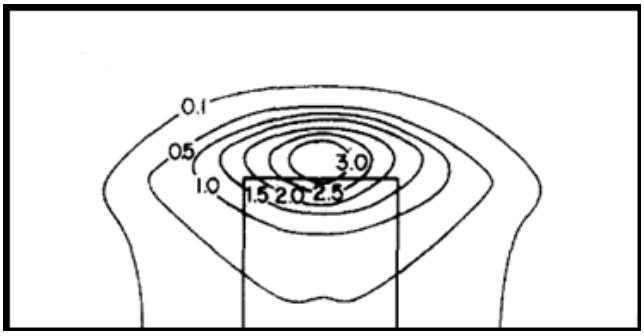

Figure 2.5 Two dimensional perspective behind the building of the pollutant concentration K with vent located at the rooftop's centre (Figure 2.4(b)) (adapted from [7])

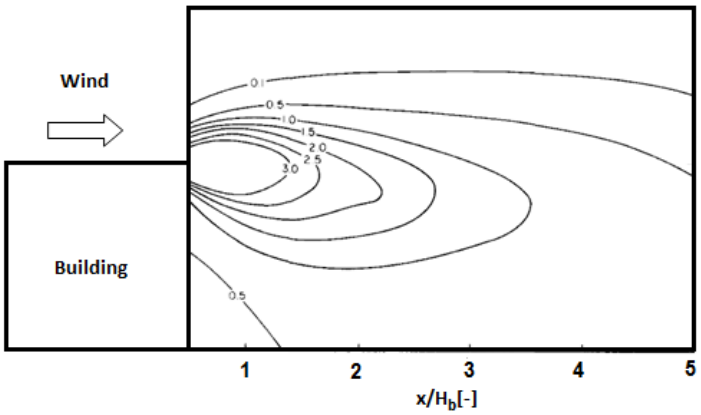

Figure 2.6 Side perspective of the pollutant concentration K behind the building with vent located at the rooftop's centre (Figure 2.4(b)) (adapted from [7])

The concentration of pure helium was quantified by the dimensionless concentration coefficient K obtained through the following equation and shown by isolines in Figure 2.4-2.6:

$$K = \frac{c U_b {H_b}^2}{Q_e} \quad (10)$$

K: dimensionless concentration coefficient [-]

c: mass fraction of the pollutant [-]

U_b: wind velocity at reference building height H_b [m/s]

H_b: building height [m]

Q_e: emission rate of the pollutant [m^3/s]

Table 2.2 Parameters for defining the computational domain [7]

Parameter	Description	Value
α	power-law exponent [-]	0.19
H	domain height [m]	0.30
H_b	building reference height [m]	0.05
U_b	mean velocity in x-direction at reference height H_b [m/s]	3.30
U_{ref}	mean wind velocity at reference height [m/s]	4.50
Q_e	emission rate of the pollutant [m^3/s]	0.0000125
z_0	Ground aerodynamic roughness length [m]	0.0000750

Some parameters for defining the computational domain and boundary conditions from Li and Meroney [7] are shown in Tabe 2.2. Figure 2.7 and Figure 2.8 show the turbulence intensity (I_u) and dimensionless wind-speed (U/U_{ref}), respectively. For numerical simulation, both profiles have been used to define the wind-speed and turbulence ones at the inlet and outlet the domain.

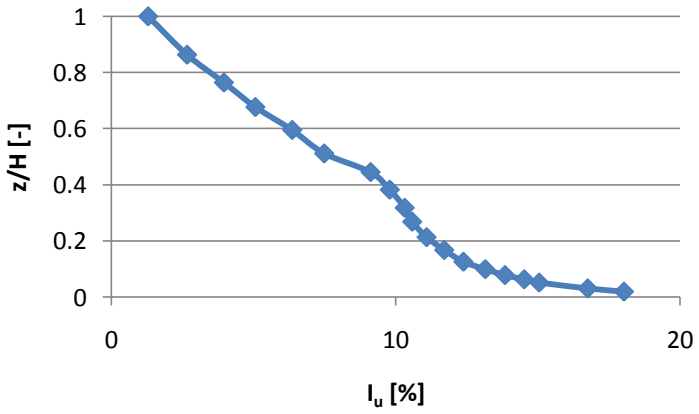

Figure 2.7 Turbulence intensity, I_u (%) (adapted from [7])

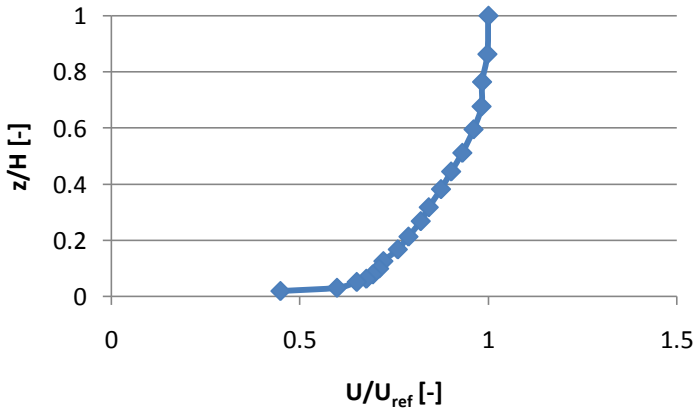

Figure 2.8 Dimensionless mean wind-speed (adapted from [7])

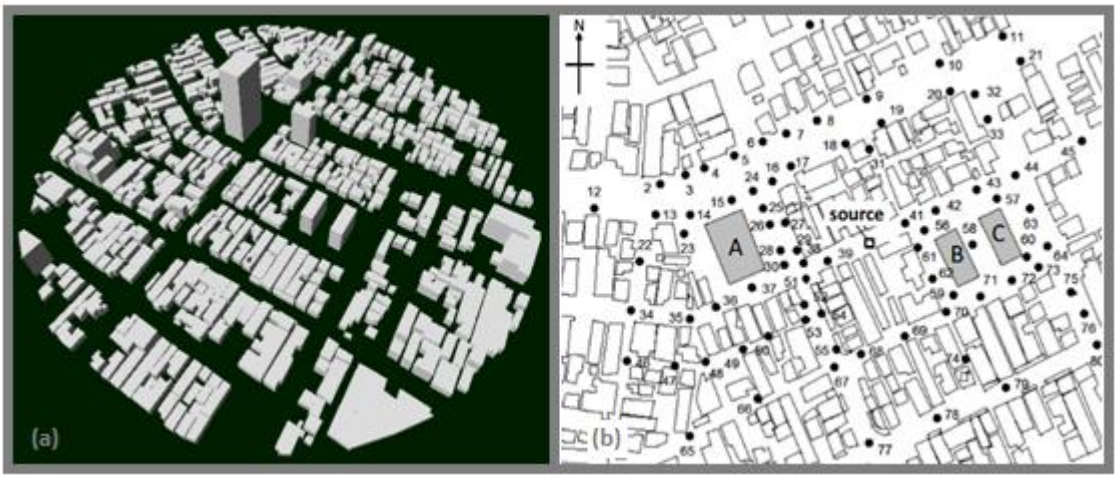

Figure 2.9 (a) Perspective view of geometry of Niigata's urban area and (b) measurement points location [8-10]

Tominaga et al. [8] developed wind-tunnel experiments using a reduced-scale model of an actual urban area of Niigata city, Japan. A perspective view of geometry of that urban area is presented in Figure 2.9 (a). Measurements of the wind flow field were conducted in eighty reference locations distributed in the urban environment as shown by Figure 2.9 (b). The wind flow field was measured 0.008 m high at reduced-scale which means 2 m at full-scale aiming to perform those measurements at the pedestrian-level.

For the same model configuration, the Architectural Institute of Japan (AIJ) [9] set a pollutant source releasing ethylene (C_2H_4) near the centre of the urban area. Then, measurements for both wind flow (Figure 2.10) and pollutant concentration field (Figure 2.11) were conducted quantifying the pollutant concentration by using concentration coefficient K already focused in the experiments of Li and Meroney [7]. Measurements were performed for four wind directions without modifications on the model. Those results presented in Figure 2.10-2.11 were measured from west wind direction.

.

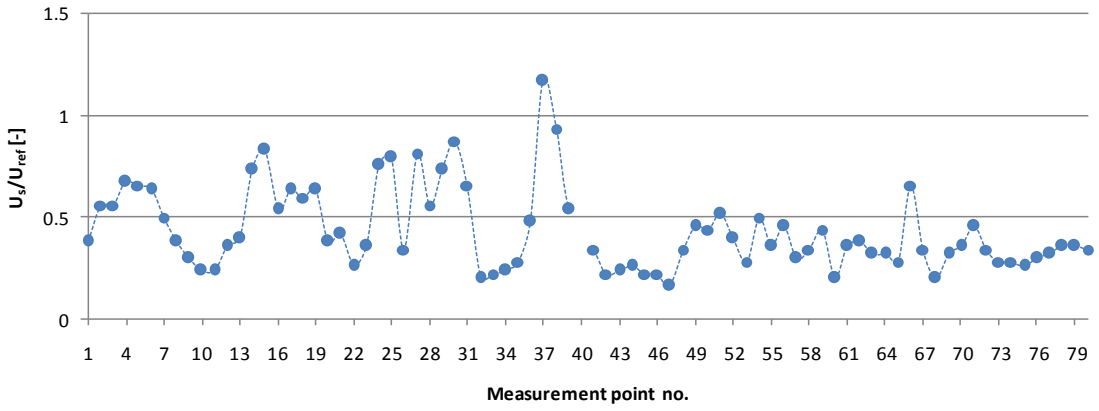

Figure 2.10 Wind flow field (data provided by AIJ)

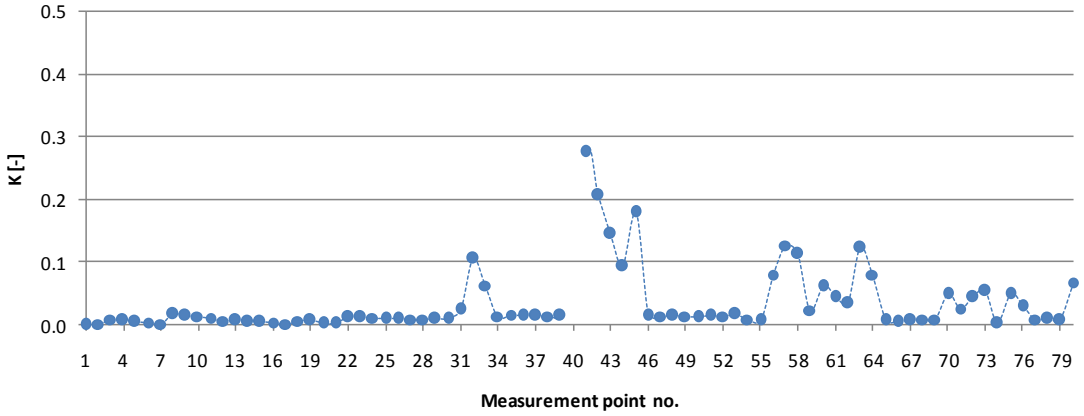

Figure 2.11 Concentration K (data provided by AIJ)

2.3.2 Numerical studies

All the wind-tunnel experiments previously referred [7,8] have provided results that are able for validating results of CFD simulations conducted with similar model configuration (Figure 2.12).

Many authors [6, 17-20] have based on experimental measurements [7] for predicting the pollutant concentration in a similar isolated cubic building by using CFD simulation, testing the sensibility of those results with several turbulence models and different pollutant source positions.

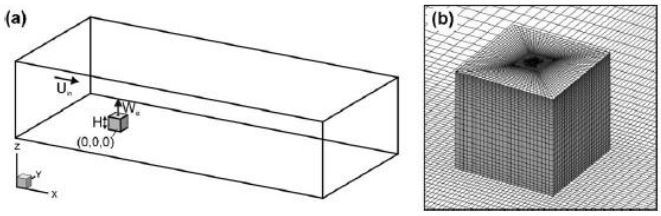

Figure 2.12 From the case study 2 performed by Gousseau et al. [6]. (a) Computational domain; (b) grid view (total number of cells: 1,480,754)

The most part of the authors [6, 17-20] have focused into analyse recirculation of the wind flow on the rooftop of the building as shown in Figure 2.13. That recirculation can cause backflow opposite the wind direction as consequence of the vortices on the rooftop, sides and behind the building (Figure 1.2-1.4). Recirculation and backflow are warnings for the reinjection of pollutants to inside the buildings and their high amount of concentration around the buildings at the pedestrian-level. High quantities of air pollution are harmful for the human's well-being, influencing his health and productivity negatively.

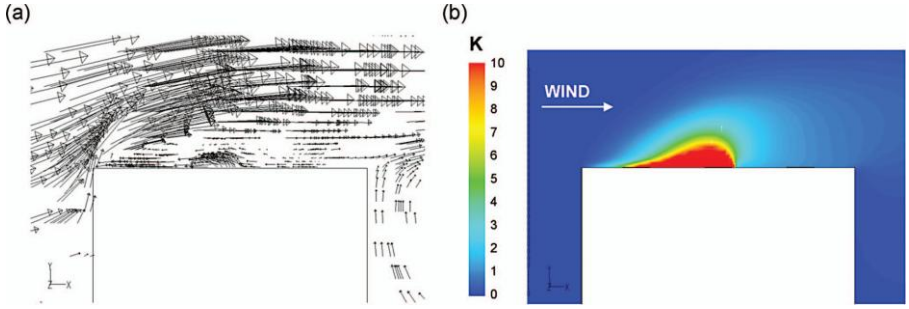

Figure 2.13 Side perspective of the vent at the rooftop's centre. (a) Wind-speed and recirculation of the flow (b) Pollutant concentration K going on the opposite direction of the wind flow because of the backflow promoted by the recirculation on the rooftop [1]

Numerical simulation results of the pollutant concentration on the rooftop and behind the building are shown in Figure 2.14-2.16.

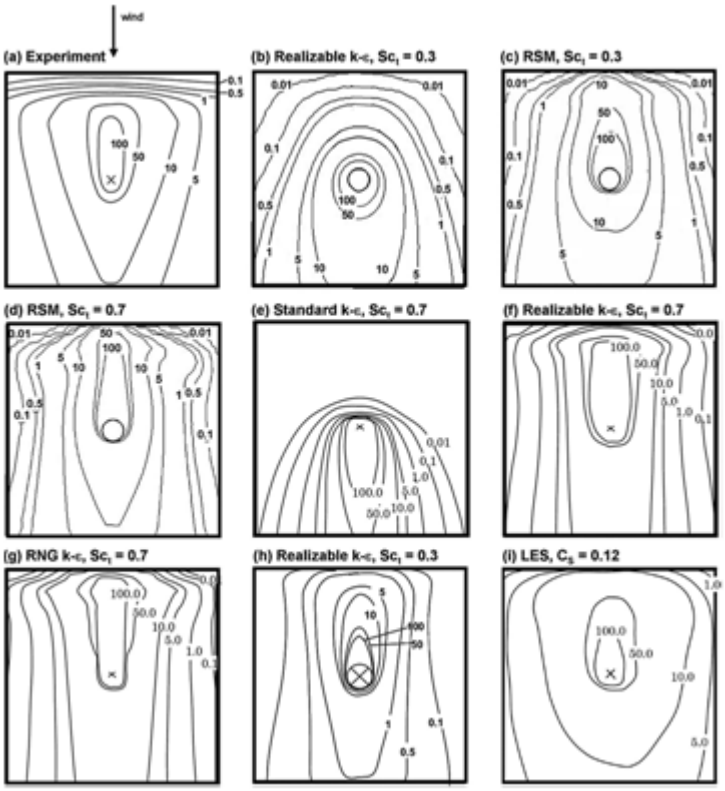

Figure 2.14 Pollutant concentration K on the rooftop: (a) Wind-tunnel measurements by Li and Meroney [7]. (b-i) CFD results by: (b-d) Wang [17]; (e-g) Tominaga and Stathopoulos [18]; (h) Blocken et al. [19]; (i) Tominaga and Stathopoulos [20]. Results are presented for different turbulence models and turbulent Schmidt numbers, Sc_t. C_S is the roughness constant [1]

Some cases were not able for reproducing recirculation on the rooftop because the turbulence model's limitations as shown in Figure 2.14 (e). Other cases can reproduce recirculation with different level of precision. The turbulent Schmidt number significantly influences some turbulence k-ε models as shown by a side-by-side comparison between both Figure 2.14 (f) and Figure 2.14 (h). The turbulence model approach has also a big influence on the results with special attention to Figure 2.15 (f) and 2.16 (f) that both resulted from LES simulation.

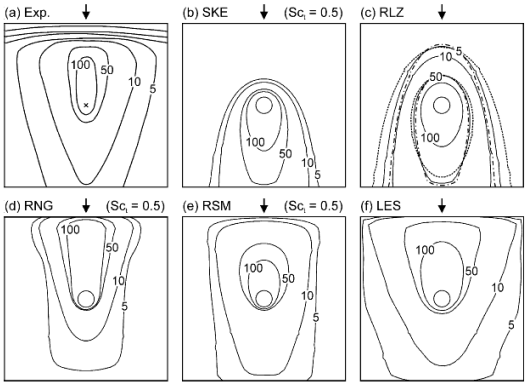

Figure 2.15 (a) Experimental [7] and (b-f) numerical contours of the pollutant concentration K [6]

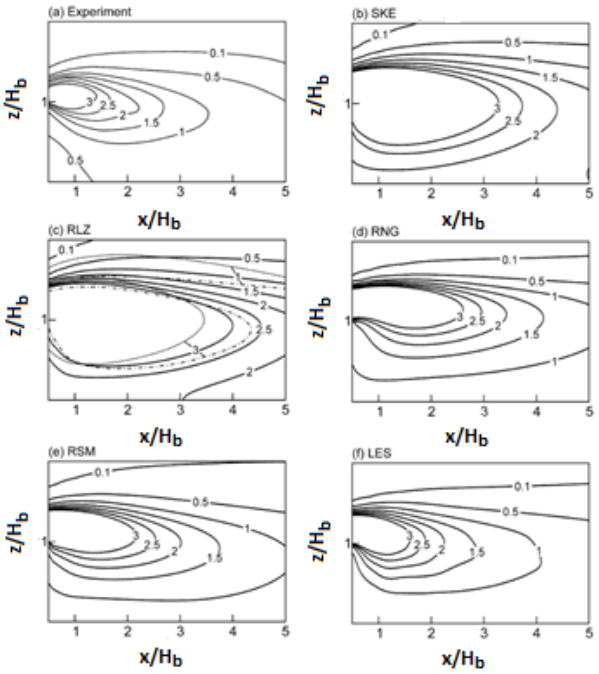

Figure 2.16 Side perspective of the pollutant concentration K behind the building (a) for the experiments conducted by Li and Meroney [7] and (b)-(f) for different turbulence models performed by Gousseau et al. [6]

CFD simulation has been conducted to predict pollutant concentration in urban areas as well. The study of the downtown of Montreal, Canada, was conducted by Stathopoulos et al. [21] through a reduced-scale model and, more recently, Gousseau et al. [22] have performed CFD simulation for the same model configuration which are validated with such results from Stathopoulos et al. [21].

A side-by-side comparison between reduced-scale models and grid arrangements is being presented in Figure 2.17 and Figure 2.18, for both southwest (SW) and west (W) wind direction.

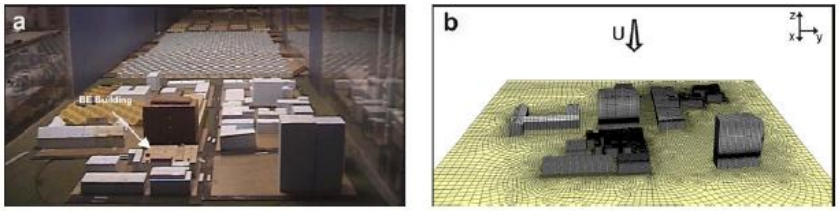

Figure 2.17 Side-by-side comparison between both southwest wind-tunnel model and computational domain [22]

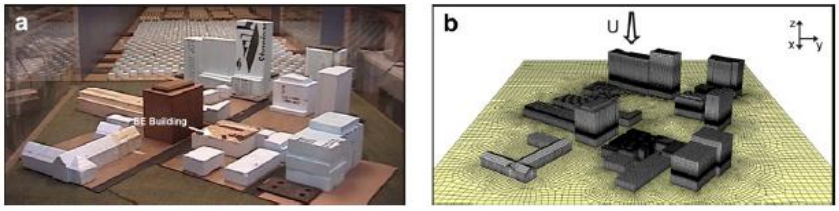

Figure 2.18 Side-by-side comparison between both west wind-tunnel model and computational domain [22]

Measurements and predictions were made for fifteen reference positions as presented in Table 2.3. Pollutant concentration is quantified to hundred times the concentration coefficient K (100K). Several turbulence models were focused and a sensibility analysis of the turbulent Schmidt number was made with the Standard k-ε model.

Table 2.3 Dimensionless concentration (100K) and relative error values at each measurement point for the southwest direction [22]

Point No.	100K (EXP)	Standard k-ε model Sc_t=0.3		Standard k-ε model Sc_t=0.5		Standard k-ε model Sc_t=0.7		LES	
		100K	%error	100K	%error	100K	%error	100K	%error
1	27	20.2	25.2	13.4	50.4	7.7	71.5	12.6	53.3
2	32	32.7	2.2	23.9	25.3	15.1	52.8	16.2	49.4
3	57	70.1	23.0	53.9	5.4	34.3	39.8	27.8	51.2
4	71	69.7	1.8	62.3	12.3	50.0	29.6	32.7	53.9
5	60	125.5	109.2	104.2	73.7	78.6	31.0	47.8	20.3
6	104	174.2	67.5	124.0	19.2	68.8	33.8	38.1	63.4
7	68	62.4	8.2	68.5	0.7	66.9	1.6	30.5	55.1
8	96	90.5	5.7	91.6	4.6	84.3	12.2	42.1	56.1
9	131	1972.8	1406.0	797.7	508.9	365.2	178.8	227.3	73.5
10	79	59.5	24.7	74.0	6.3	81.7	3.4	31.3	60.4
11	69	73.5	6.5	82.5	19.6	87.8	27.2	40.0	42.0
12	120	77.7	35.3	70.6	41.2	69.2	42.3	43.1	64.1
13	59	77.1	30.7	37.9	35.8	23.2	60.7	52.4	11.2
14	925	314.3	66.0	624.2	32.5	858.3	7.2	439.7	52.5
15	1050	354.0	66.3	548.2	47.8	596.0	43.2	327.2	68.8

The concentration level of pollutants around the source are shown through Figure 2.19 for the southwest wind direction experiments. Differences between the turbulence models occur in respect to the pollutant concentration distribution, however recirculation of the wind flow is reproduced with both. The correlation between experimental and predicted results is quantified through the plots presented in Figure 2.20 with fair agreement.

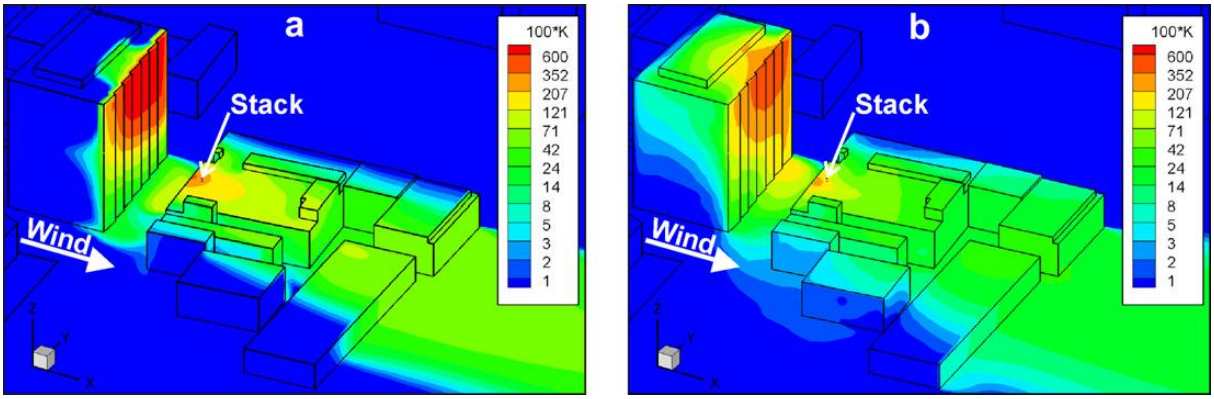

Figure 2.19 Contours of the pollutant concentration 100K near the source for the southwest direction obtained with (a) Standard k-ε model (Sc_t = 0.7) and (b) LES [22]

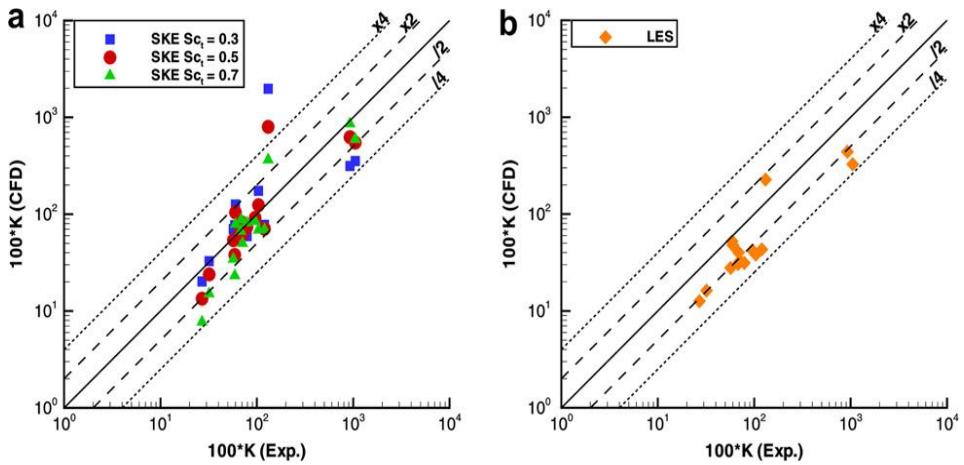

Figure 2.20 Correlation of 100K for the southwest results by using (a) Standard k-ε model and (b) LES in comparison with experiments [22]

2.4 Quantification of agreement between the results

Aiming to quantify the agreement between experimental (E) and predicted (P) results are proposed the following statistical factors FB, NMSE, FAC2 and R [23]. N indicates the total amount of data, i the index of the value in the data and σ_E and σ_p the standard deviation of experimental (E) and predicted (P) values respectively.

$$FB = \frac{\bar{E}-\bar{P}}{0.5(\bar{E}+\bar{P})} \tag{11}$$

$$NMSE = \frac{\overline{(E_i-P_i)^2}}{\bar{E}\bar{P}} \tag{12}$$

$$FAC2 = \frac{1}{N}\sum_{i=1}^{N} n_i \rightarrow n_i = \begin{cases} 1, & 0.5 \leq \frac{P_i}{E_i} \leq 2 \\ 0, & else \end{cases} \tag{13}$$

$$R = \frac{[(E_i-\bar{E})(P_i-\bar{P})]}{\sigma_E \sigma_P} \tag{14}$$

Fractional Bias (FB) quantifies systematic errors while Normalized Mean Square Error (NMSE) both the systematic and unsystematic ones. The ideal value is set to be zero which means no errors at all.

Fraction of Predictions within a factor of 2 of observations (FAC2) quantifies the number of data that is inside the range [0.5;2] considered acceptable for the ratio between predictions (P) and experimental results (E). Thus, in a perfect scenario FAC2 would be one meaning one hundred per cent of data inside the range. The correlation coefficient (R) consists in the linear relationship for both predicted (P) and experimental (E) results. R would also be one in a perfect scenario.

3. Case 1: Pollutant dispersion around an isolated cubic building

3.1 Experimental setup

3.1.1 Description

Li and Meroney [7] created a reduced-scale model of an isolated cubic building with a rooftop vent releasing pure helium (he). Several wind directions and distinct vent positions on the rooftop have been tested aiming to measure the pollutant concentration field. Results focus the influence of those different wind directions and distinct vent positions on the rooftop recirculation of the wind flow (Figure 2.4) and recirculation behind the building. (Figure 2.5-2.6). The concentration of pure helium was quantified by using the dimensionless concentration coefficient K (10).

3.1.2 Results

Figure 2.4 show a significant level of recirculation on the rooftop which forms backflow opposite the wind direction. Behind the building, Figure 2.5-2.6 present lower concentration than on the rooftop. Indeed, at the pedestrian-level behind the building, concentration level is becoming lower.

3.2 CFD simulations

Case 1 aims to predict both the wind flow and pollutant concentration field which involves an isolated cubic building with a rooftop vent releasing pure helium (he). From west wind direction, several RANS turbulence models are tested. Predictions from Case 1 will be validated by comparisons against the wind-tunnel measurements from Li and Meroney [7] whose model configuration and input conditions are the base of the present case study.

Generally, numerical simulations with RANS equations require less computational resources and time than simulations with LES. Therefore, simulation with RANS has been conducted to generate an overview of the prediction accuracy of that turbulence model approach for the pollutant dispersion around isolated cubic buildings. The geometry is based on the experimental setup was performed by Li and Meroney [7] and previously presented. Those experiments have been used by different authors to assess the accuracy of numerical simulations in predicting pollutant concentration and to test the influence of the boundary conditions or other relevant parameters such as the wind direction, rooftop vent location or influence of the turbulent Schmidt number Sc_t [1,6,7].

The numerical assessment of the pollutant concentration will start by sizing the computational domain and creating a quality grid arrangement. Then, different turbulence k-ε models will be tested modeling first by using the RNG k-ε model. Predictions for both the turbulence Realizable k-ε model and RSM model will be also conducted. Based on the experimental setup and in the spatial discretization of the computational domain will be set the wind-speed and turbulence profiles and the boundary conditions. The west wind direction and a building configuration with a vent at the centre of the rooftop will considered in the present case study.

3.2.1 Model and computational domain

Computational domain from Case 1 is being displayed below in Figure 3.1. The wind-speed profile is represented by the arrows coming from the west direction.

For sizing the computational domain, minimum ranges of distance from their boundaries to the cubic building were respected in order to achieve a computational domain wide enough to limit influence on the wind flow around the building [11,12]. The building's height H_b is set to 0.05 m [7]. Building was then placed five times H_b far from inlet, top and sides of the domain, and twenty times

far from outlet of the domain. At the centre of the rooftop pure helium is being released from a circular exhaust vent.

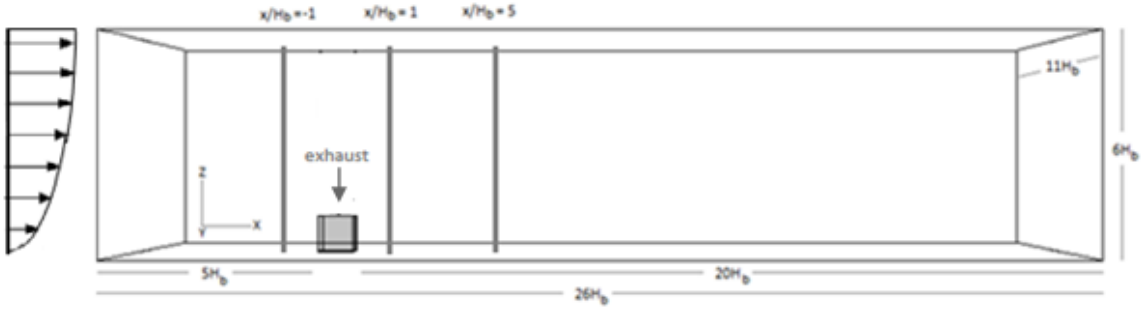

Figure 3.1 Computational domain from Case 1. x/H_b indicates domain planes.

3.2.2 Computational grid

The spatial discretization of the computational domain should achieve a quality grid arrangement which can be assessed through the grid attributes skewness and stretching ratio. Based on those attributes, a quality grid was arranged with a total amount of 518,532 cells. It was made with the pre-processor Gambit 2.4.6.

All the domain was extruded from the ground-level up to the domain's height established ($6H_b$). Then, the internal volume of the building (Figure 3.2) were entirely deleted from the ground-level to the building's height (H_b) in order to set it as a wall [14].

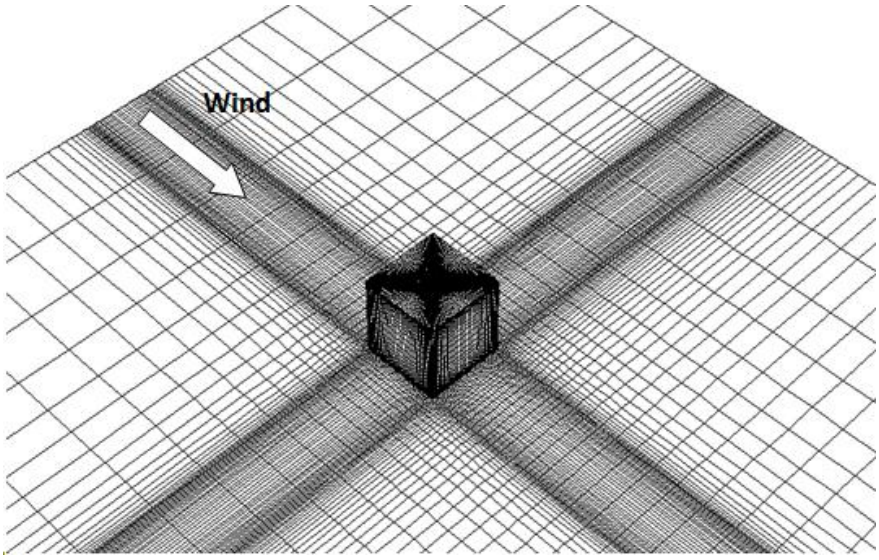

Figure 3.2 Perspective view of part of the grid arrangement from Case 1. Wind direction is indicated by the arrow (518,532 cells).

The circular rooftop vent arranged on the rooftop's face was modeled as a velocity inlet. Around it, 180 cells were defined in order to mesh the internal part of the vent. This is the finest meshed part of the entire domain.

Part of the computational grid is presented by Figure 3.2. Also fine mesh was arranged near the roof, front, side and back wall where the wind flow separation and recirculation occurs (Figure 1.2-1.4) [11,12].

Both Figure 3.3 and Figure 3.4 show Gambit perspective views of the grid arrangement. Figure 3.5 shows that grid in the internal part of the rooftop vent (a), and the quality of the cell's shape

(b) in a qualitative scale from 0 to 1 in which 0 is the best cell and 1 is the worst one. From those Figure 3.5 (a) and (b), it is possible to observe that, in general, inside and around the rooftop vent is being provided a quality grid arrangement.

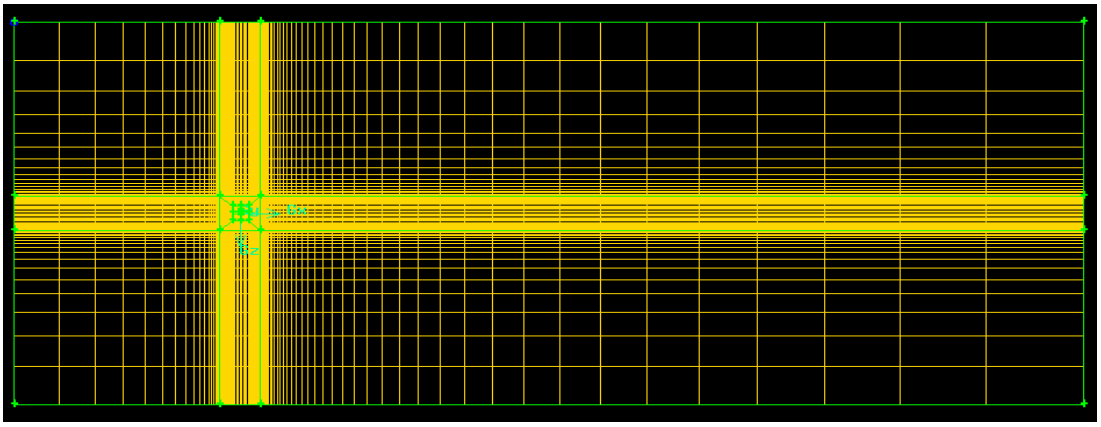

Figure 3.3 Horizontal section of the computational domain

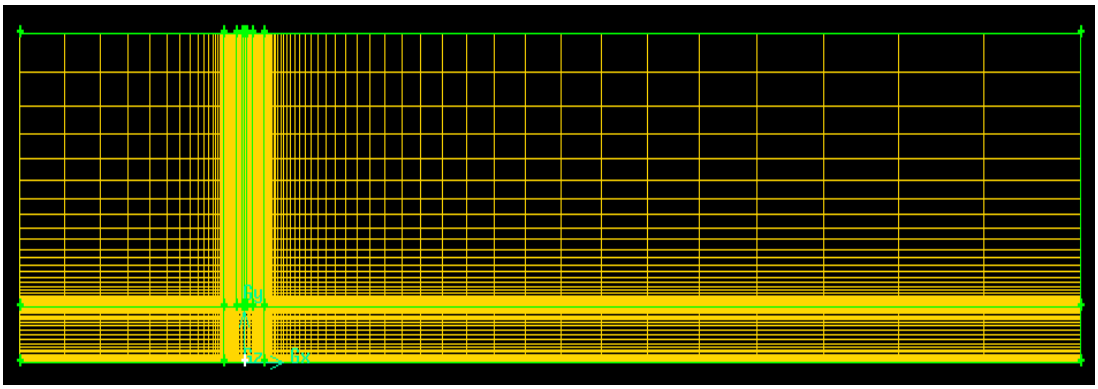

Figure 3.4 Vertical section of the computational domain

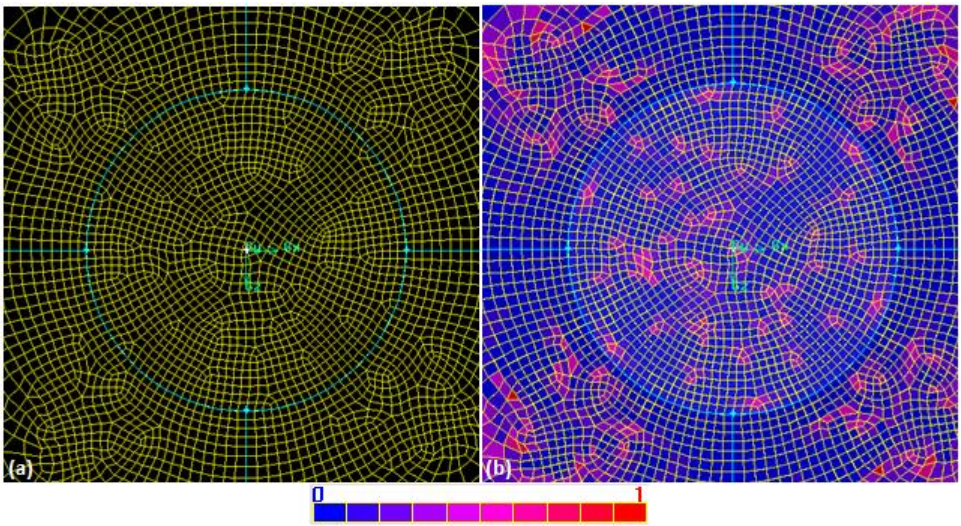

Figure 3.5 Rooftop vent perspectives: (a) standard grid view; (b) quality of the cells' shape through a qualitative scale between 0 and 1 (blue-red scale) in which 0 is the best element and 1 the worst one

3.2.3 Boundary conditions

Before initializing any simulation, conditions should be set for characterizing the domain boundary conditions at the inlet, outlet, bottom, top and side walls. Also the rooftop vent, top and side walls of the building require boundary conditions for defining the pollutant released and turbulence associated to the source's geometry. Those boundary conditions were defined as expressed in Table 3.1.

Table 3.1 Boundary conditions from Case 1

Inlet	Velocity inlet
	Momentum: Velocity magnitude U(z)
	Turbulence: k(z), ε(z)
Outlet	Pressure outlet
	Static/Gauge pressure (Pa): 0
	Turbulence: k(z), ε(z)
Bottom	Wall, Shear condition: no slip
	Wall roughness: z_0=0.000075 m, C_s>1 (UDF: C_s=3.7), k_S = 0.00020 m
Top	Symmetry
Side Walls	Symmetry
Rooftop vent	z-velocity: 0.627 m/s
	Turbulence: Intensity and Length scale
	Turbulence intensity: 11.8%
	Turbulence length scale: 0.00035 m
	Species: helium; Mass fraction: 1
Top and side walls of building	Wall
	Shear condition: no-slip
	Wall roughness: k_s=0.0m; C_s=0.5

The wind flow and turbulence profile at the inlet and outlet are based on the measurements of the mean wind-speed and turbulence intensity (Figure 2.7-2.8) from Li and Meroney [7]. The wind flow was obtained by multiplying the mean wind-speed U/U_{ref} (Figure 2.7) by U_{ref}. The turbulent kinetic energy k was calculated by the following equation as function of the domain's height [12] from the turbulence intensity I_u (Figure 2.8):

$$k(z) = (I_u(z)U(z))^2 \quad (15)$$

The turbulence dissipation rate ε(z) was imposed at the inlet through a user-defined function (UDF) from the equation (6) (see Annex I). The Von Kárman constant, κ, was set to 0.42 and the friction velocity, u*, was established 0.22 m/s, according to previous studies using the same geometry. The wind flow and turbulence profile are then presented in Figure 3.6-3.8. Also a set of relevant parameters presented in Table 3.2 was used from the experimental setup for calculating the boundary conditions.

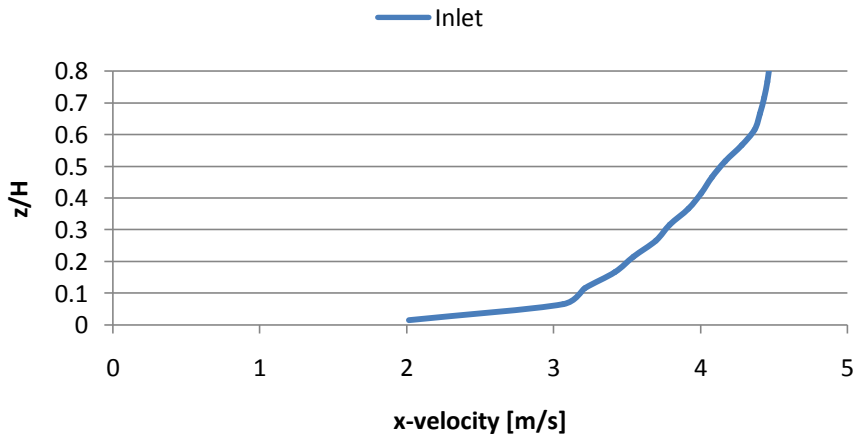

Figure 3.6 Mean wind velocity at the inlet from Case 1

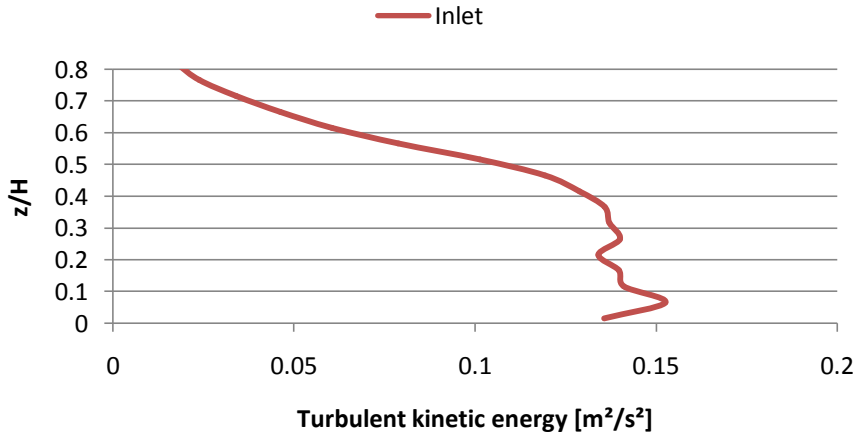

Figure 3.7 Turbulent kinetic energy at the inlet from Case 1

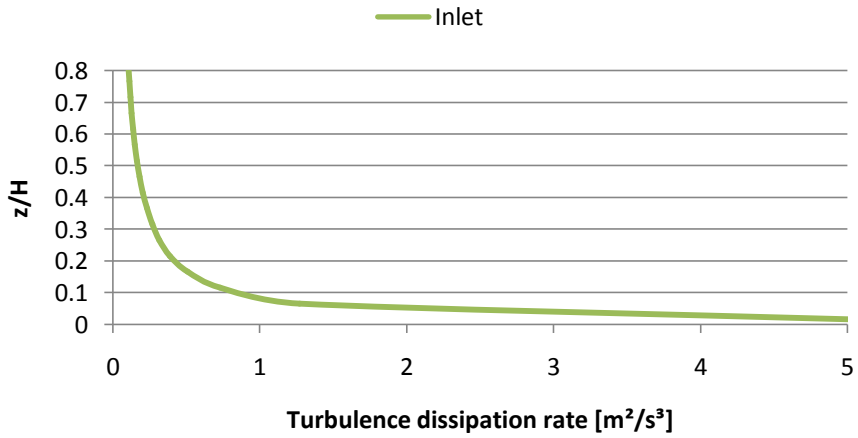

Figure 3.8 Turbulence dissipation rate at the inlet from Case 1

Table 3.2 Model parameters for calculating the boundary conditions

Parameter	Description	Value
α	Power-law exponent	0.19
H_b	Building reference height [m]	0.05
D_v	Exhaust diameter [m]	0.005
U_H	Mean velocity in x-direction at reference height H_b [m/s]	3.30
W_e	Exhaust velocity [m/s]	0.627
M_e	Exhaust momentum ratio	0.19
A_v	Exhaust surface [m²]	0.00002
Q_e	Emission rate of the pollutant [m³/s]	0.00001

At the bottom were defined both wall shear condition (no slip) and wall roughness. Wall roughness requires definition of the surface roughness length z_0 and the roughness constant C_s. z_0 has been set by Li and Meroney [7] and it has also been used by other authors for the presented model configuration [6,17-20]. However, C_s directly depends on the grid arrangement. Then, it is possible to calculate C_s by using equation (8) and the statement $k_s<y_p$ [13,16]. k_s is the physical roughness height of the bottom and y_p corresponds to half the height of the grid first cell. Therefore, y_p was set to 0.00023 m and k_s equal to 0.00020 m for assuring that relationship $k_s<y_p$. From (8) C_s is set to 3.7. As $C_s> 1$, an user-defined function (UDF) for setting the value of the constant C_s is required because it is out of the range [0;1] (see Annex 1) [16]. Both the top and side walls of the computational domain were set as symmetry which means no boundary conditions were defined at these planes because there is no flux of any quantity [13].

The rooftop vent was modeled by defining an exhaust vertical velocity, W_e, the turbulence intensity and length scale and the pollutant (pure helium). W_e was defined through the momentum ratio M_e [7]. M_e is equal to 0.19 and is a ratio between the exhaust vertical velocity W_e and the velocity at the reference height which means building's height 3.3 m/s. Then, W_e was set to 0.627 m/s.

The turbulence intensity I_u, which is a measured value at the inlet boundary, has been stated by Li and Meroney [7] to 11.8%. The turbulence length scale L_t was set 0.07 times the rooftop vent diameter [13] from equation (9).

Top and side walls of the building were set to default walls keeping the shear condition and wall roughness as recommended [13].

3.2.4 Other relevant parameters and settings

Besides the boundary conditions, discretization schemes have to be selected in spite of their influence in RANS simulations is smaller. Those schemes are presented in Table 3.3. Generally, second-order scheme is able to achieve higher accuracy than the first-order one [13]. The maximum degree of convergence was set to 10^{-11} for all the variables.

Table 3.3 Discretization schemes

Discretization	Pressure-velocity coupling: SIMPLE (Semi-Implicit Method for Pressure-Linked Equations)
	Pressure: Second order
	Momentum, k and ε: Second order upwind
	Helium, Energy: Second order upwind

3.3 Comparison experiments with simulations

A side-by-side comparison between the experimental and predicted results of the Case 1 will be presented. Also the "case study 2" from Gousseau et al. [6] will be focused for comparison once it was treated the same building model configuration.

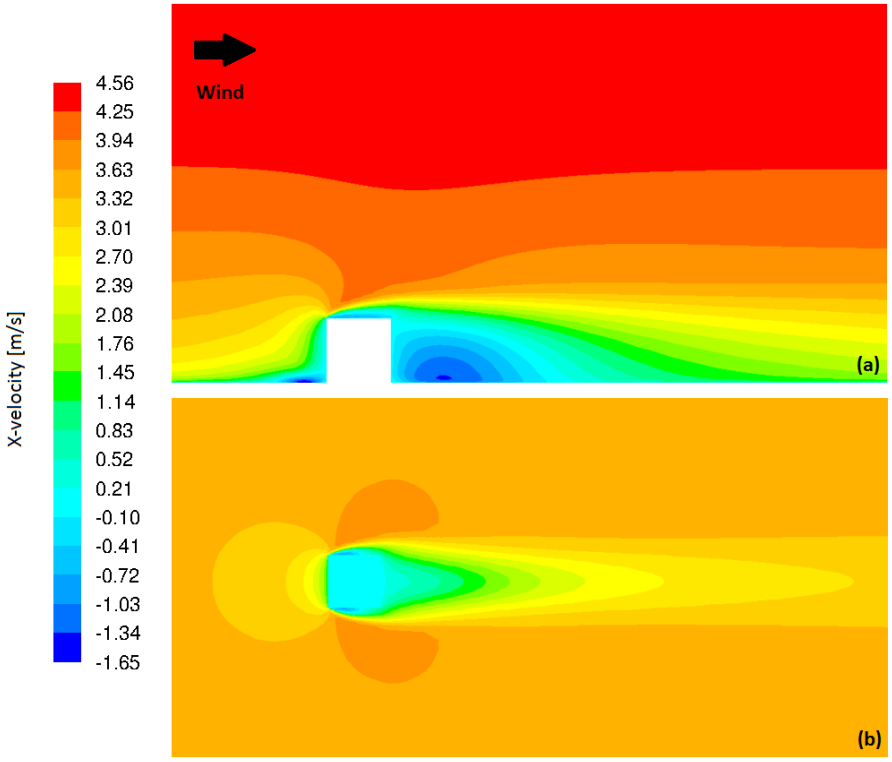

Figure 3.9 Case 1: X-velocity (a) vertical plane (side view) and (b) horizontal plane (top view)

Results from Case 1 are then reported. Figure 3.9 shows the velocity contours in the x-direction for both vertical (a) and horizontal perspective (b). It is possible to identify the wind flow separation zone and stagnation region in front of the building, recirculation on the rooftop, sides and behind the building by comparing Figure 3.9 (a) against Figure 1.2-1.4. Recirculation causes backflow opposite the wind direction as demonstrated by the experimental results in Figure 3.10 (a). Predicted results [6] present fair agreement against the experiments, in spite of overpredicted.

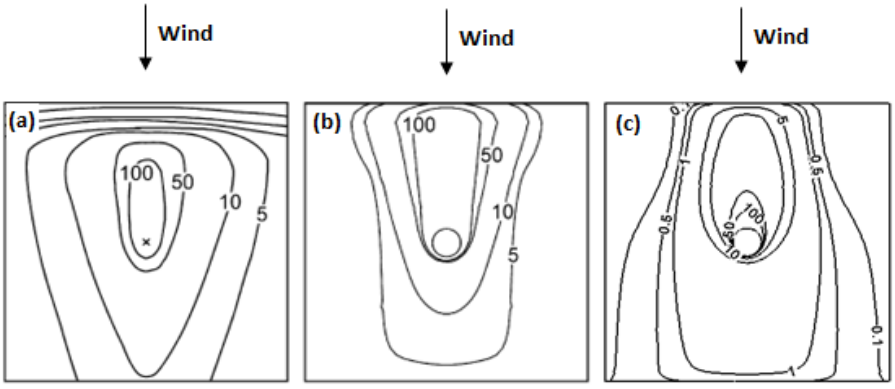

Figure 3.10 Concentration contours on the rooftop (a) by Li and Meroney [7], (b) by Gousseau et al. [6] and (c) from Case 1. Both (b) and (c) were calculated by using RANS RNG k-ε model.

From Case 1, pollutant concentration contours on the rooftop are significantly underpredicted in relation to the experimental setup [7]. However, recirculation of the flow is clear on the rooftop Figure 3.10 (c).

Pollutant concentration predictions were also performed at the pedestrian-level, behind the building as shown in Figure 3.11. Case 1 still reproduces concentration levels with significant underprediction at this region (Figure 3.11(a)). In general, Gousseau et al. [6] overpredicted them in Figure 3.11 (b), however their results show better agreement to the experiments (Figure 3.11(c)) than the ones provided by Case 1.

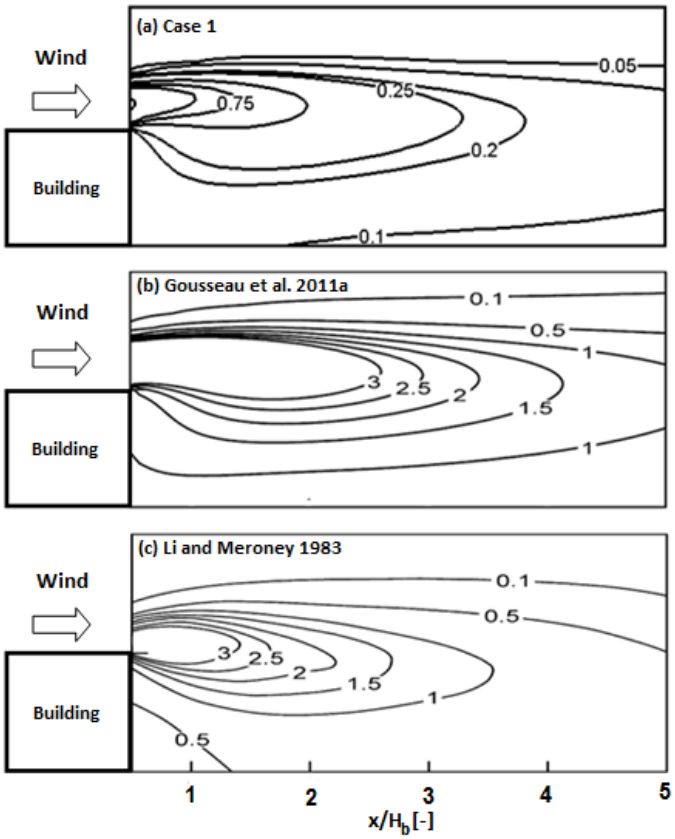

Figure 3.11 Pollutant concentration K contours at the pedestrian-level behind the building (a) from Case 1, (b) by Gousseau et al. [6] and (c) by Li and Meroney [7]. Both (b) and (c) was calculated by using RANS RNG k-ε model.

Figure 3.12-3.15 corroborate the underprediction of those results shown previously. The plots presented only provide comparisons between Case 1 and the experimental measurements since Gousseau et al. [6] do not provide such results. Figure 3.12 analyse the pollutant concentration at the ground-level behind the building. This region was already focused in Figure 3.11 for analysing concentration in heights higher than the ground. Now, observing the ground-level results, values are not changing significantly which means that Case 1 is still underpredicted.

Pollutant concentration on the top edge behind the building at $x/H_b=1$ (Figure 3.13) show fair agreement between Case 1 and the experiments. However, between $y/H_b=-05$ and $y/H_b=0.5$, mainly in the centre ($y/H_b=0$) this agreement becomes poor. Here, pollutant concentration predictions are substantially underpredicted from measured value of 3 to a predicted one of 0.5 (Case 1 prediction).

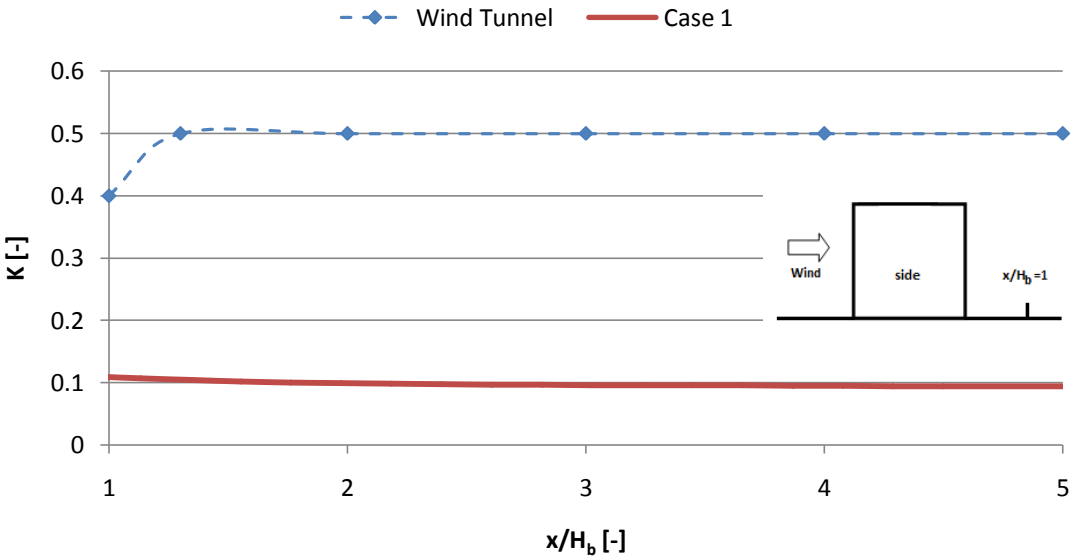

Figure 3.12 Pollutant concentration K predictions at the ground-level behind the building

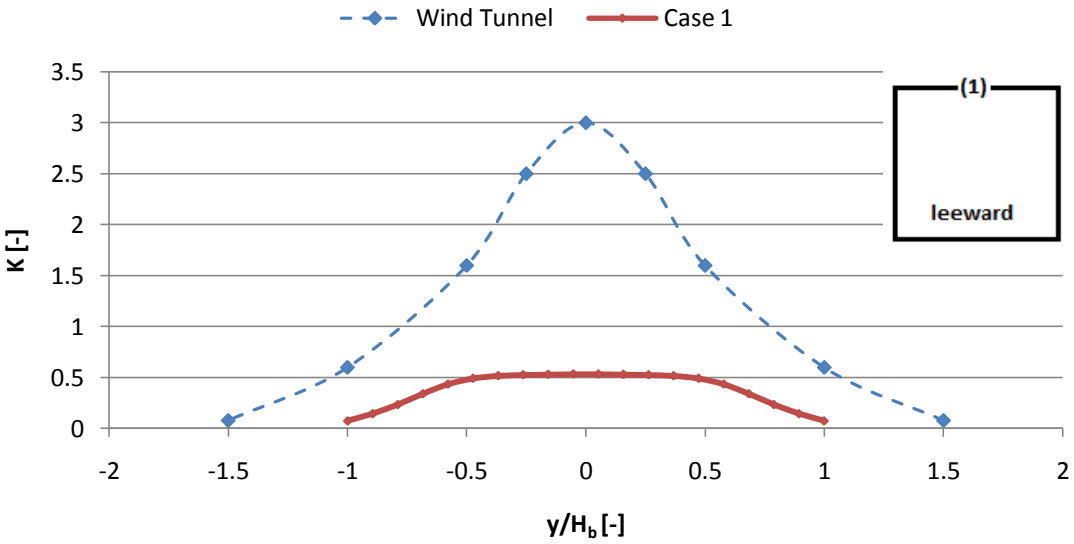

Figure 3.13 Pollutant concentration K predictions in the edge (1) behind the building at $x/H_b=1$

On the boundaries of the building, pollutant concentration is analysed as well. Based on the numerical study [19] both rooftop and back's centreline are on focus (Figure 3.14-3.15). On the rooftop, recirculation level is slightly underpredicted and not that gradual as should be based on the experimental results. Concentrations change suddenly from 660 ($x/H_b=0$) to 100 ($x/H_b=-0.12$). From wind-tunnel experiments, concentration level 100 is achieved on the rooftop's centerline at $x/H_b=-0.31$. On the back's centreline behind the building, pollutant conentration predictions are underpredicted, mainly between $z/H_b=0.6$ and $z/H_b=1.0$.

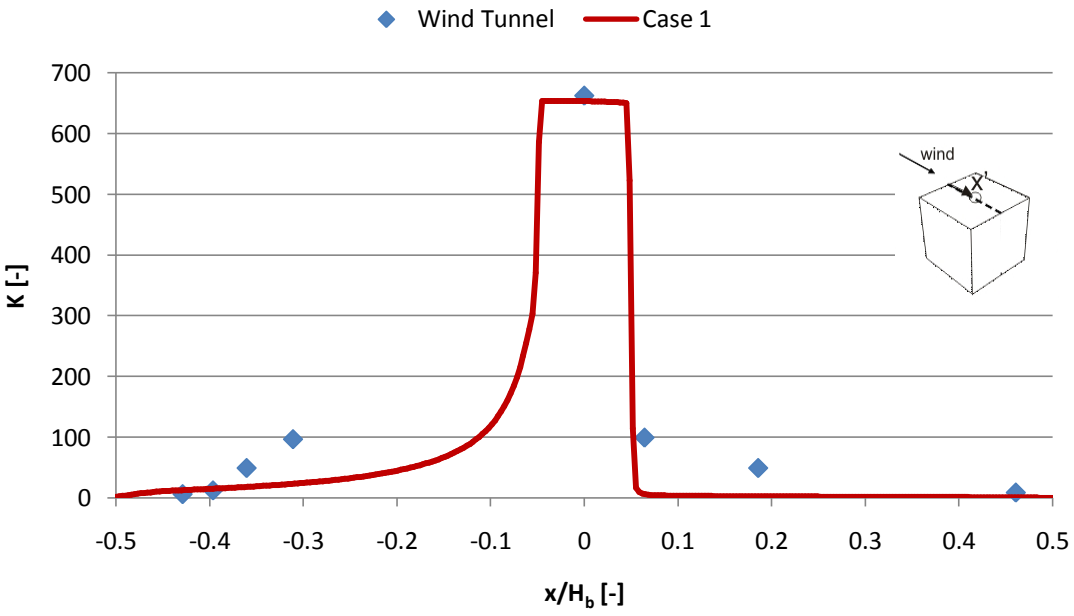

Figure 3.14 Pollutant concentration K on the rooftop's centreline

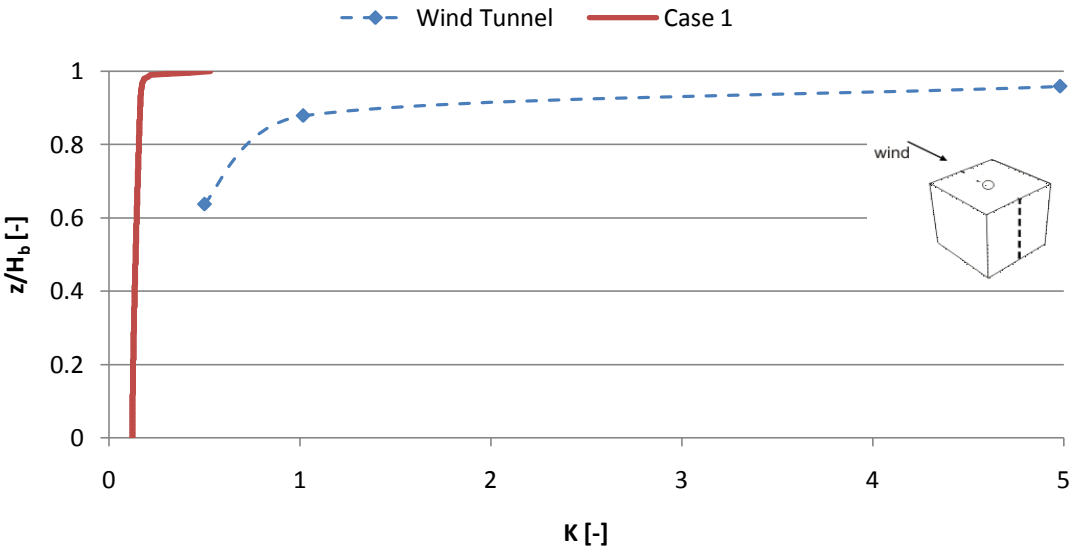

Figure 3.15 Pollutant concentration K on the back's centreline behind the building

3.4 Sensitivity analysis

3.4.1 Grid-sensitivity

It is recommended that the grid-sensitivity should be tested in order to guarantee that results do not change significantly with more or less cells for the same model configuration [11,12]. Therefore, a grid-sensitivity analysis was performed increasing the total amount of cells. As recommended by Franke et al. [11] and Tominaga et al. [12], a factor of √2 was set to increase the

number of cells that compose every single edge. Then, the finest grid achieved a total amount of 1,701,080 cells. A comparison between both coarser and finer grid can be made by observing Figure 3.16. After performing simulations by using the turbulence RNG k-ε model for both grids and using the same boundary conditions as well, it was concluded that those results did not change significantly. Thus, the coarsest grid was selected for performing new simulations with different turbulence models.

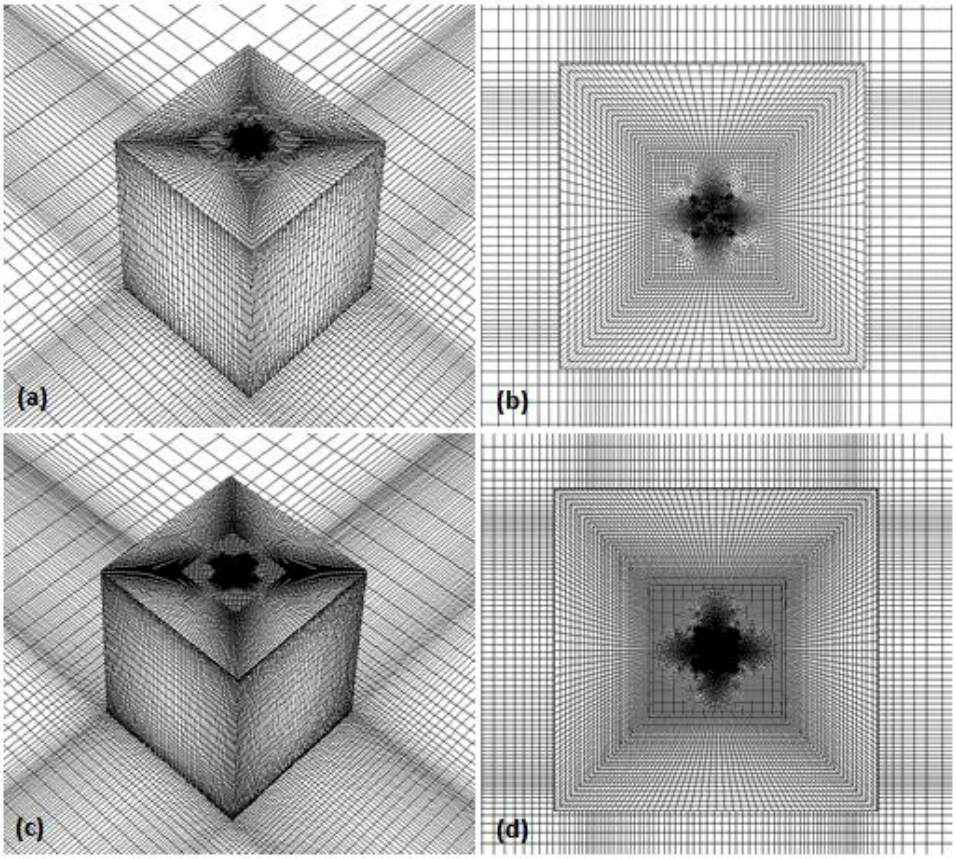

Figure 3.16 Grid arrangements: Coarse grid 518,532 cells (a-b) and Fine grid 1,701,080 cells(c-d); (a) and (c) show the side, back and top of the building; (b) and (d) show a closer top view of the building

In general, there is no large discrepancies between both coarser and finer grid. Pollutant concentration contours on the rooftop (Figure 3.17) and behind the building (Figure 3.18-3.19) have shown fair agreement.

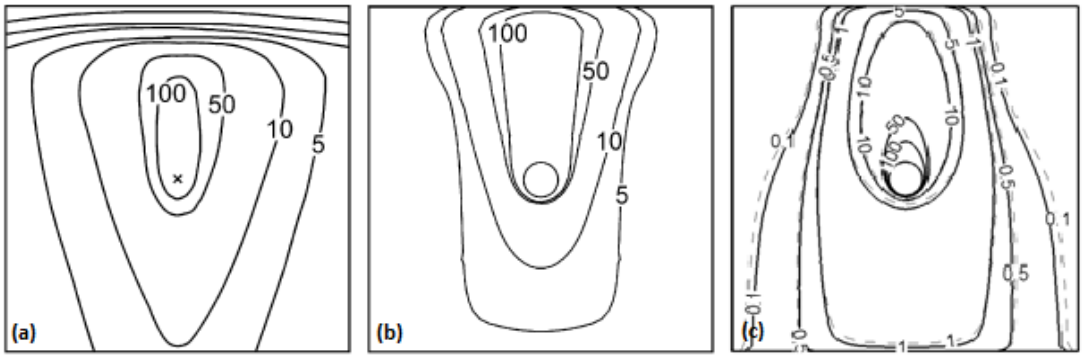

Figure 3.17 Concentration contours on the rooftop: (a) Experimental results by Li and Meroney (1983); (b) CFD results by Gousseau et al (2011a); (c) Case 1 (continuous line – coarse grid; dashed line – fine grid)

Some discrepancies occur behind the building at the building's height as shown in Figure 3.20. Mainly in the range $-0.5<y/H_b<0.5$, H_b far the building, the finest grid show higher levels of concentration than the coarsest one which means more accuracy when comparing against the experimental results presented through Figure 2.5. Both pollutant concentration predictions on the rooftop's and back's centreline show no discrepancies (Figure 3.21-3.22). As the coarsest grid requires less time-consuming, it was selected for testing more turbulence models. Those results will be presented in the following sections.

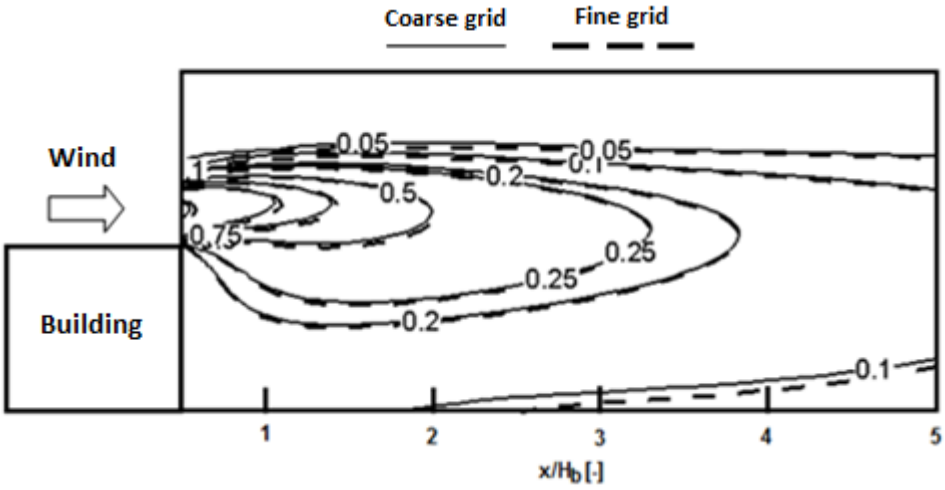

Figure 3.18 Comparison of pollutant concentration K contours behind the building. Continuous line is the coarsest grid; Dashed line corresponds to the finest grid.

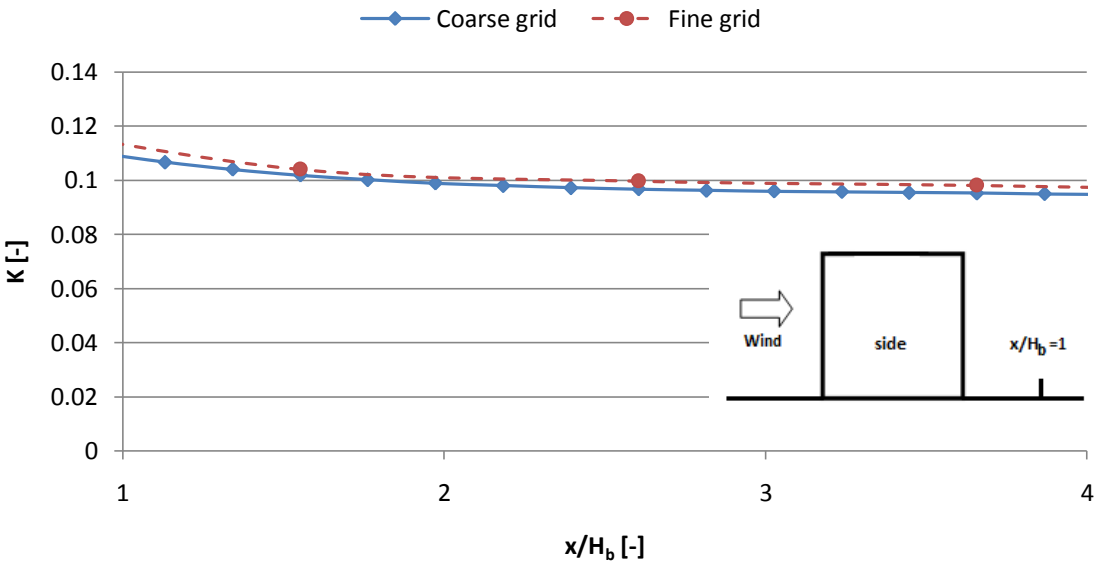

Figure 3.19 Comparison of pollutant concentration K predictions at the ground-level behind the building

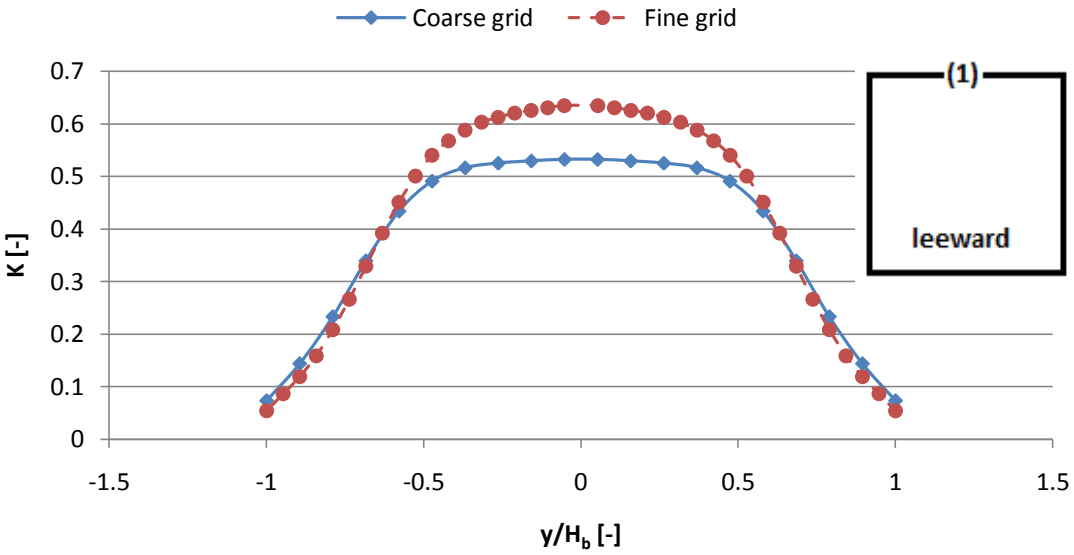

Figure 3.20 Comparison of pollutant concentration K predictions in the edge (1) behind the building at $x/H_b=1$ (H_b far the building)

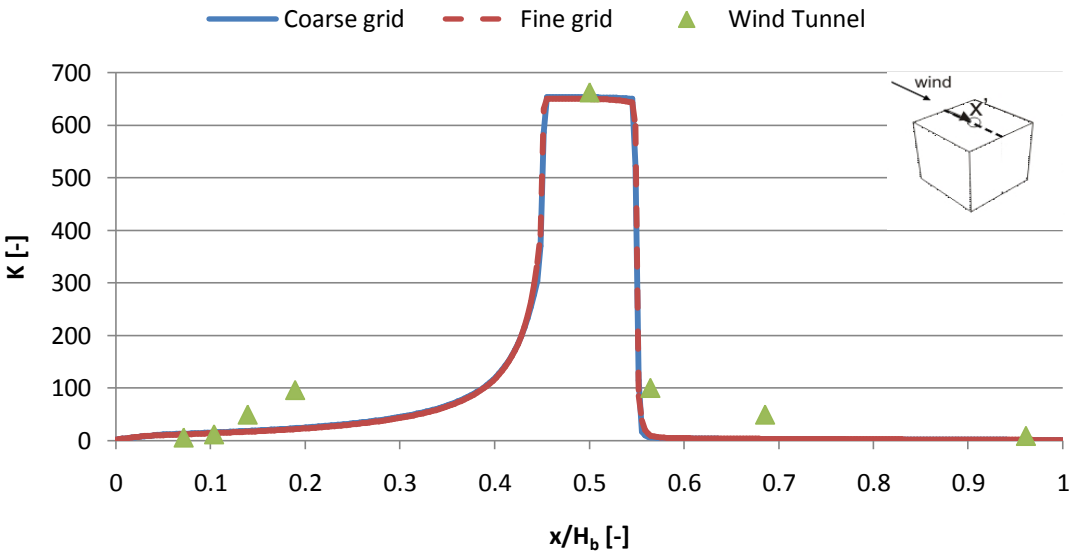

Figure 3.21 Comparison pollutant concentration K on the rooftop's centreline

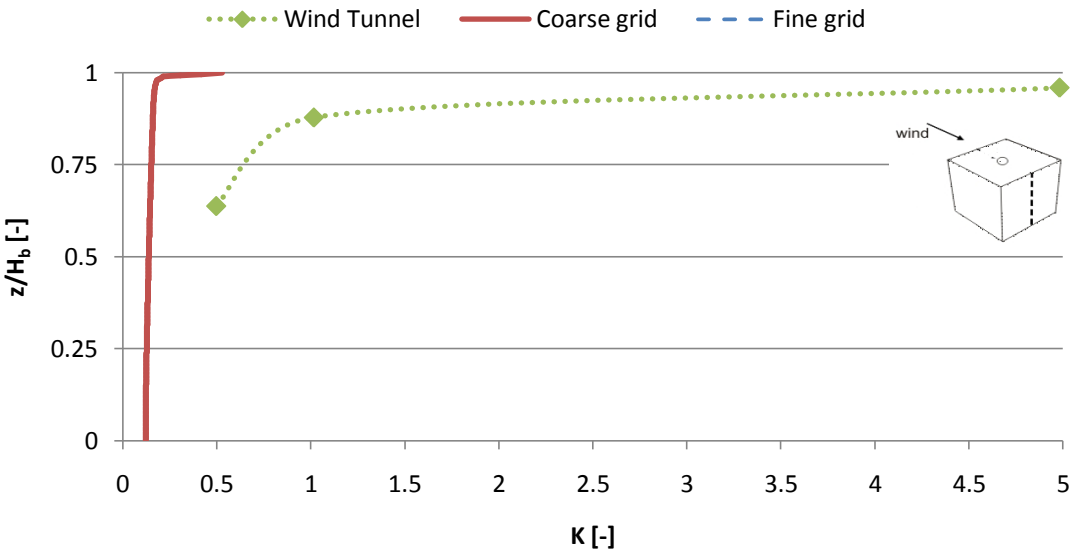

Figure 3.22 Comparison of pollutant concentration K on the back's centreline behind the building

3.4.2 Influence of turbulence models: RNG k-ε model, Realizable k-ε model and RSM

In the previous section, it was presented results simulating with RANS by using the turbulence RNG k-ε model. Two more RANS turbulence models were tested, the Realizable (RLZ) k-ε model and Reynolds-stress model (RSM). The calculation conditions are similar with the RNG k-ε model. With the Realizable k-ε model the turbulent Schmidt number (Sc_t) was set to 0.7. Thus, comparison with numerical results provided by Gousseau et al. [6] can be done against simulations from Case 1 once such turbulence models, both the wind flow and turbulence profiles and boundary conditions are all similar. Those results are compared through Figure 3.23-3-29 by presenting pollutant concentration contours on the rooftop (Figure 3.23), behind the building (Figure 24-27) and in both rooftop's centreline (Figure 3.28) and back's centreline behind the building (Figure 3.29).

In general, from Case 1, all the turbulence models achieved underpredicted results in relation to the simulation results from Gousseau et al. [6] and the experimental setup [7].

On the rooftop and at the ground-level behind the building, Case 1 presents fair agreement between the three turbulence models in respect to the pollutant dispersion patterns (Figure 3.23-27), in spite of the underprediction already demonstrated against both numerical and experimental results provided [6,7].

In the pollutant concentration predictions H_b far behind the building (Figure 3.27), RLZ k-ε model offers the best prediction when compared against the experiments [7]. Figure 3.27 shows that both RNG k-ε model and RSM present results significantly underpredicted in relation to RLZ k-ε model and experiments [7].

In spite of good agreement presented in Figure 3.27, RLZ k-ε model have not been able to reproduce recirculation opposite the wind direction on the rooftop. Both RNG k-ε model and RSM are more accurate at that point as shown in Figure 3.28. Pollutant concentration on the back's centreline behind the building is more accurately predicted by the RLZ k-ε model near the top of the building (Figure 3.29) once again, however it is not that significant. Nevertheless, all turbulence models are still underpredicting the pollutant concentration, in spite of correctly reproducing the pollutant dispersion patterns around the building, mainly both the RNG k-ε model and RSM.

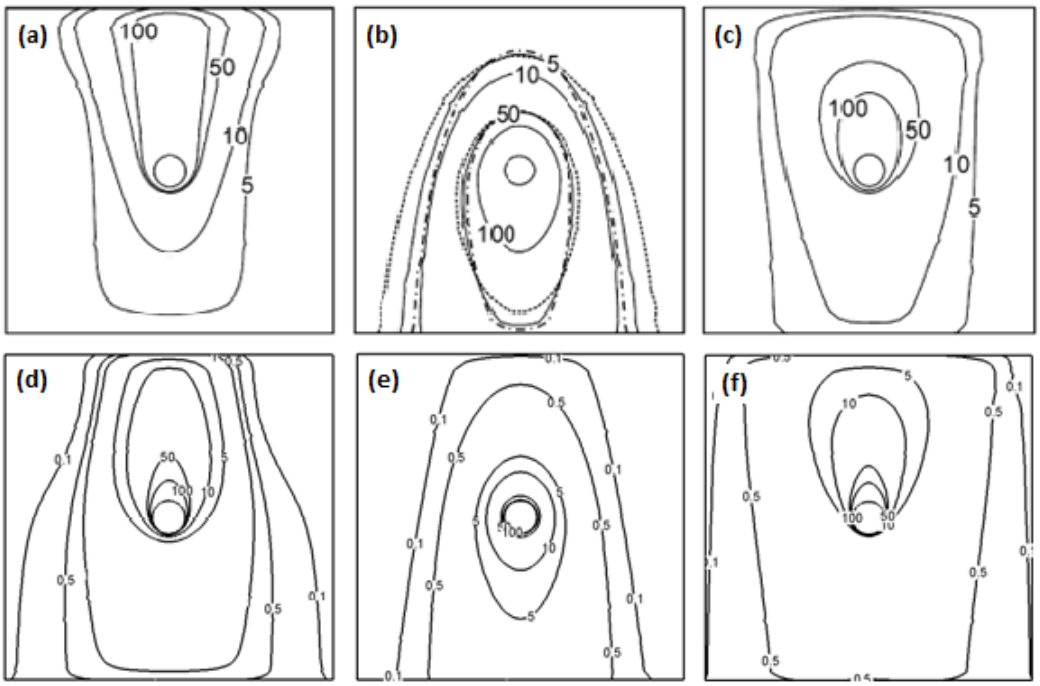

Figure 3.23 Comparison of pollutant concentration K contours on the rooftop: (a)-(c), RNG k-ε model, RLZ k-ε model and RSM from Gousseau et al. [6], respectively; (d)-(f) RNG k-ε model, RLZ k-ε model and RSM from Case 1, respectively. Note that in (b), the dash-dot line represents RLZ k-ε model with a Schimdt number of 0.7 which it is the one taken into account.

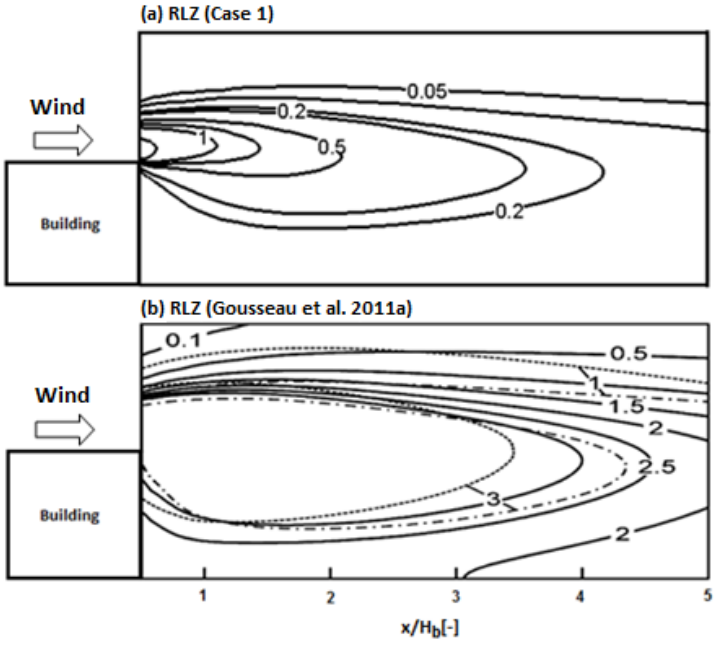

Figure 3.24 Pollutant concentration K contours behind the building (a) RLZ k-ε model from Case 1 and (b) RLZ k-ε model from Gousseau et al. [6]. Note that in (b), the dashed-dot line represents RLZ with a Schimdt number of 0.7 which it is the one taken into account.

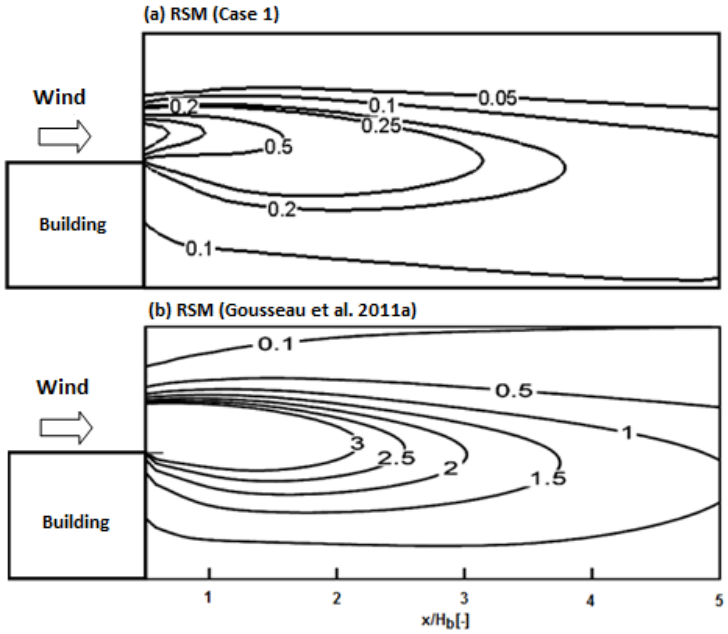

Figure 3.25 Pollutant concentration K contours behind the building (a) RSM from Case 1 and (b) RSM from Gousseau et al. [6]

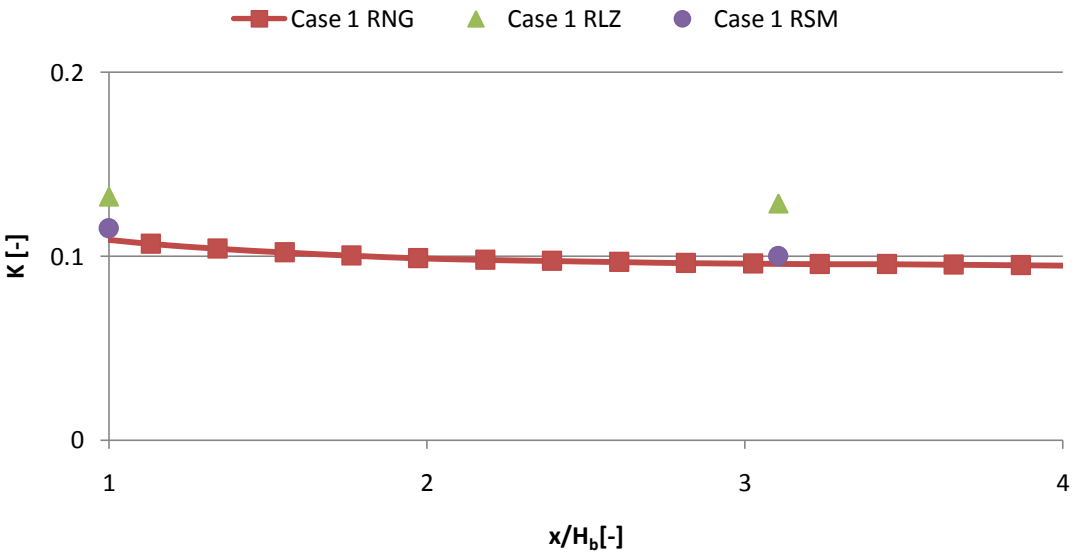

Figure 3.26 Pollutant concentration predictions at the ground-level behind the building

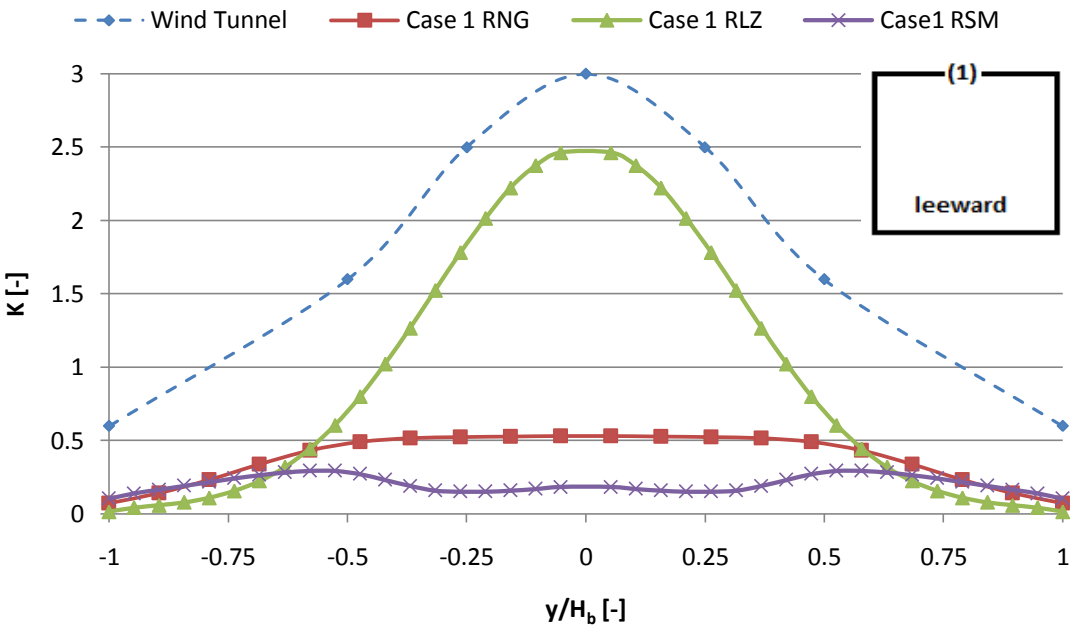

Figure 3.27 Pollutant concentration predictions in the edge (1) behind the building at $x/H_b=1$ (H_b far the building)

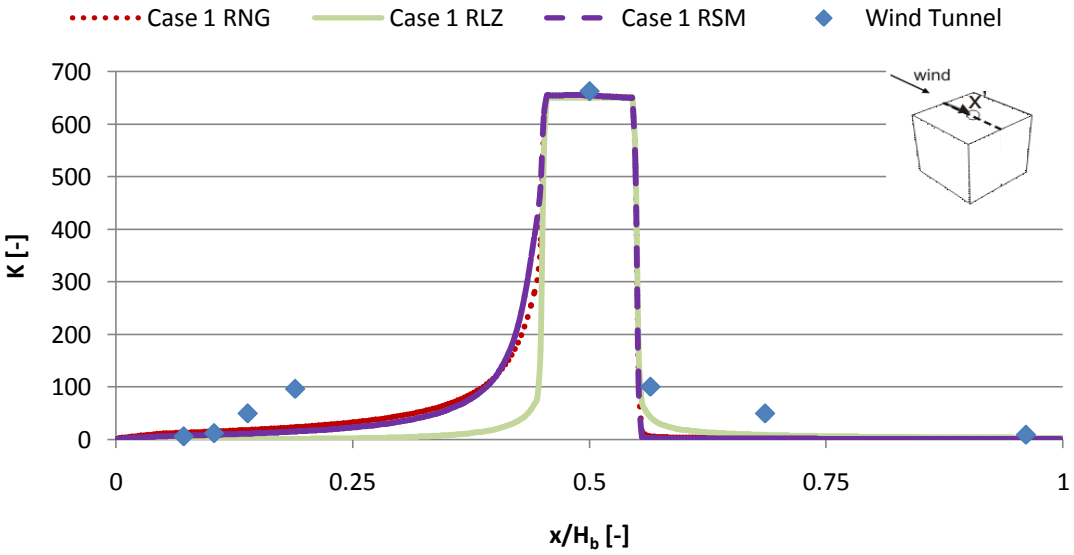

Figure 3.28 Pollutant concentration K on the rooftop's centreline

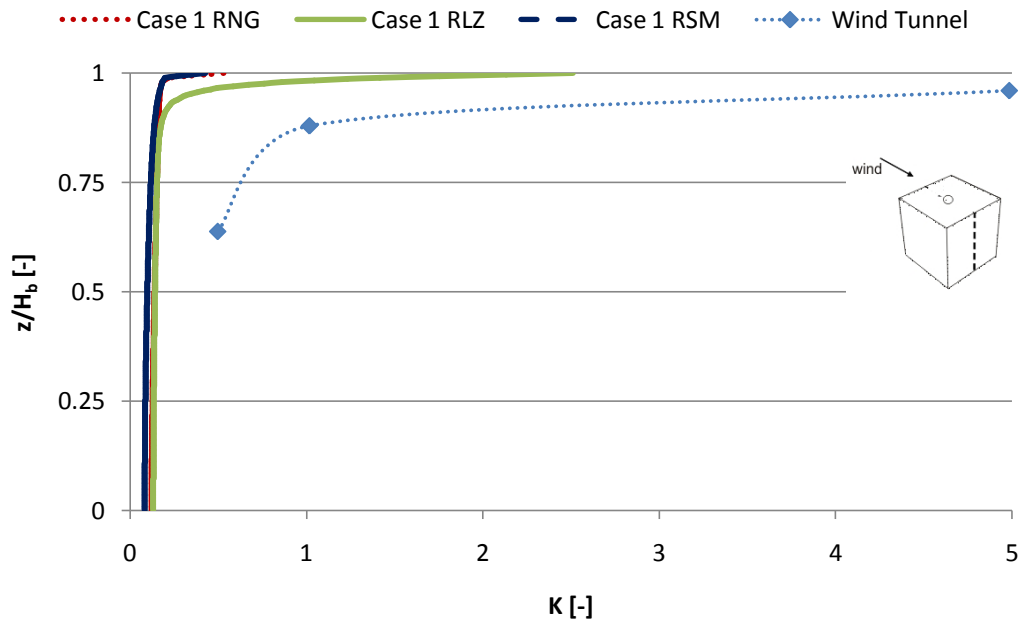

Figure 3.29 Pollutant concentration K on the back's centreline behind the building

3.4.3 Influence of turbulent kinetic energy (k)

It would be expected to achieve the same results and not such underprediction in relation to the numerical [6] and experimental results [7] from the other authors. Thus, in order to understand which kind of influence turbulence can have on the recirculation and pollutant dispersion at the rooftop level and behind the building, simulations were performed using different turbulent kinetic energy k profiles obtained by multiplying the original k values by the factors 0.25, 0.5 and 2 which means reduction of 25% and 50% and increasing of 100%. Simulations were performed with turbulence RNG k-ε model.

Figure 3.30 (a) shows the experimental pollutant concentration contours on the rooftop [7] and Figure 3.30 (b) the results obtained by Gousseau et al. [6] with the RNG k-ε model. From Case 1, by using the RNG k-ε model as well, Figure 3.30 (c)-(f) presents respectively 0.25k, 0.5k, k and 2k profiles. 0.25k presents the most accurate results and the closest ones to the numerical [6] and experimental [7] results. Also in Figure 3.31, 0.25k presents higher predictions behind the building by correctly reproducing the pollutant dispersion patterns, however their underprediction persists.

Figure 3.32 shows the pollutant concentration predictions on the rooftop's centreline as shown previously. It was clear that a considerable impact on the recirculation region exists by using different k profiles. The 0.25k profile can more accurately predict the recirculation level and pollutant dispersion values opposite the wind direction in relation to the experimental results [7]. On the other hand, the 2k profile presents the worst results. This can evidence discrepancies in the calculation of the turbulent kinetic energy k profile between both Case 1 and Gousseau et al. [6]. On the back's centreline different turbulent kinetic energy k profiles present no large discrepancies and, consequently, the agreement with the numerical [6] and experimental [7] results was not improved (Figure 3.33).

Then, it is clear that turbulent kinetic energy k has a big influence on the recirculation at the rooftop level and, there, it could have influenced the results from Case 1. In fact, with the 0.25k profile, the results provided by Gousseau et al. [6] are not better than Case 1 ones for the isolines K=50 and K=100 as shown in Figure 3.30 (a)-(c). Behind the building its influence is not that big. As expressed in Figure 3.31 and Figure 3.33, the results are not significantly improved by using different turbulent kinetic energy profiles.

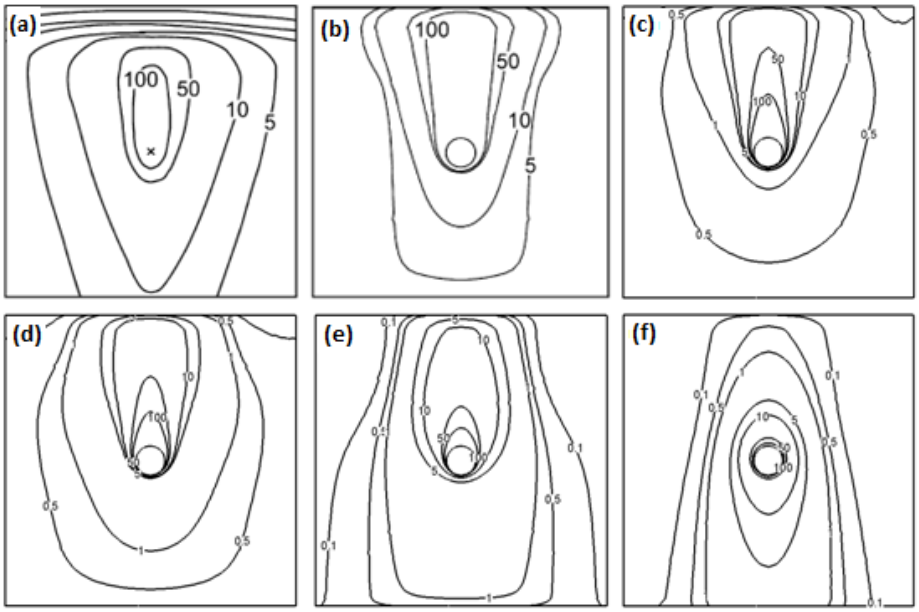

Figure 3.30 Side-by-side comparison of pollutant concentration K contours on the rooftop: (a) Experimental [7]; (b) Numerical [6]; (c)-(f) Results from Case 1 for 0.25k, 0.5k, 1k and 2k, respectively

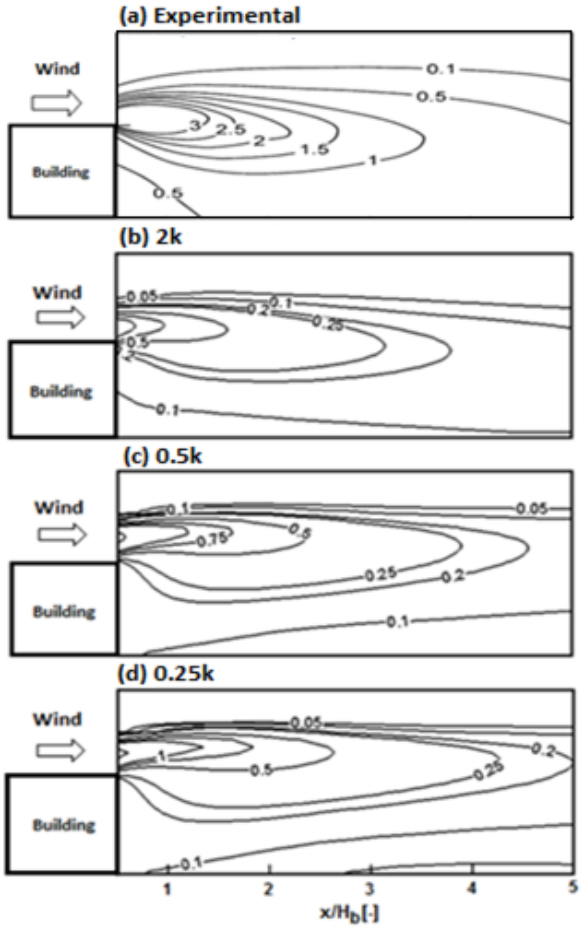

Figure 3.31 Comparison of pollutant concentration K contours behind the building: (a) Experimental [7]; (b) 2k, (c) 0.5k; (d) 0.25k

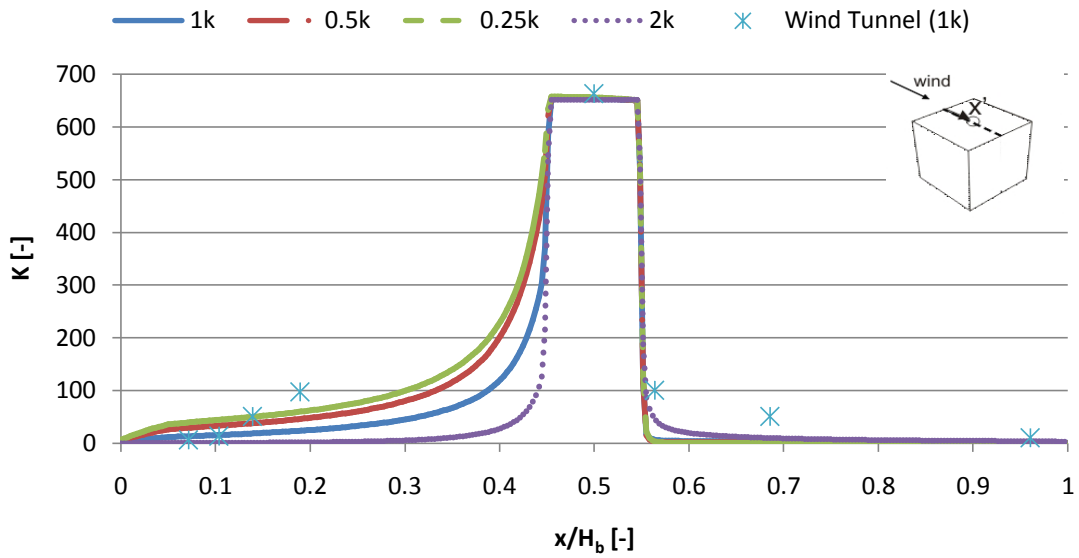

Figure 3.32 Comparison pollutant concentration on the rooftop's centreline for the several turbulent kinetic energy k profiles

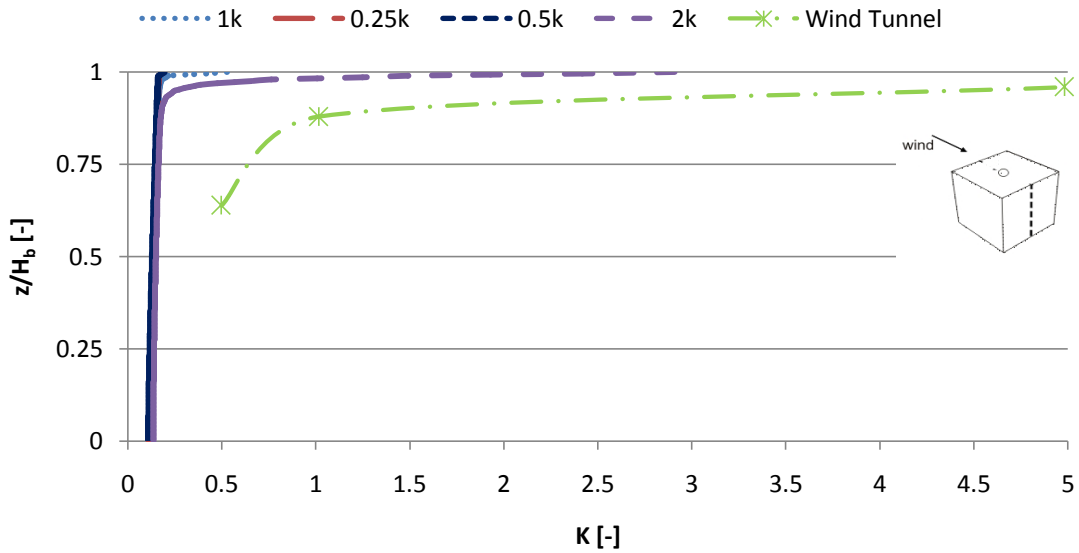

Figure 3.33 Concentration on the back's centreline behind the building for the several turbulent kinetic energy k profiles

3.5 Discussion and conclusion

Based on the previous numerical [6] and experimental [7] results for a similar model configuration, Case 1 has been developed. A computational domain sufficiently wide and a quality grid arrangement were created for simulating an isolated cubic building releasing pure helium from a rooftop vent located 0.05 m high. Also the boundary conditions were set based on those previous studies [6,7].

A grid-sensibility analysis was conducted aiming to test the influence of a higher number of cells in the simulation results achieved. As shown through Figure 3.17-3.21, the finest grid presented no large influence on the results and the coarsest one was selected to perform more simulations.

Aiming to assess the recirculation of the wind flow and pollutant concentration on the rooftop and behind the building, three turbulence models have been used such as Realizable k-ε model, RNG k-ε model and Reynolds-stresses model (RSM). The pollutant concentration was underpredicted by all of those turbulent models. However, the pollutant dispersion patterns with RNG k-ε model and RSM have presented fair agreement on both the rooftop and behind the building. This results of the accuracy of those turbulence models in predicting the recirculation, mainly on the rooftop (Figure 3.23).

Such underprediction of the results led to test kind of influence turbulence can have on the recirculation and pollutant concentration on the rooftop level and behind the building. Simulations were performed with the turbulence RNG k-ε model by using different turbulent kinetic energy k profiles obtained by multiplying the original k values by the factors 0.25, 0.5 and 2. It was concluded that lower k profiles can more accurately predict the recirculation on the rooftop while higher ones cannot, presenting worse results inclusively.

4. Case 2: Pollutant dispersion in an urban area

4.1 Experimental setup

4.1.1 Description

The Architectural Institute of Japan (AIJ) [9] developed an experimental setup using a reduced-scale model of an actual urban area of Niigata city, Japan. A perspective view of geometry of that urban area is presented in Figure 4.1. Wind-tunnel measurements of the wind flow field (Figure 2.10) were conducted in eighty reference locations distributed in the urban environment 0.008 m high at reduced-scale which means 2 m at full-scale aiming to perform those measurements at the pedestrian-level.

A pollutant source releasing ethylene (C_2H_4) was set near the centre of the urban area's model. Then, also measurements for the pollutant concentration field (Figure 2.11) were conducted quantifying the pollutant concentration by using concentration coefficient K [7]. Measurements were performed for four wind directions without modifications on the model.

The reference height was set to 15.9 m high at full-scale which means 0.064 m at reduced-scale. The ratio between the vertical exhaust velocity from the source W_s and the wind-speed at the top of the domain (momentum ratio M_s) was set to 0.5.

Three building were considered as target buildings in assessing their influence on the wind flow and pollutant concentration field, namely building A, B and C (Figure 4.1).

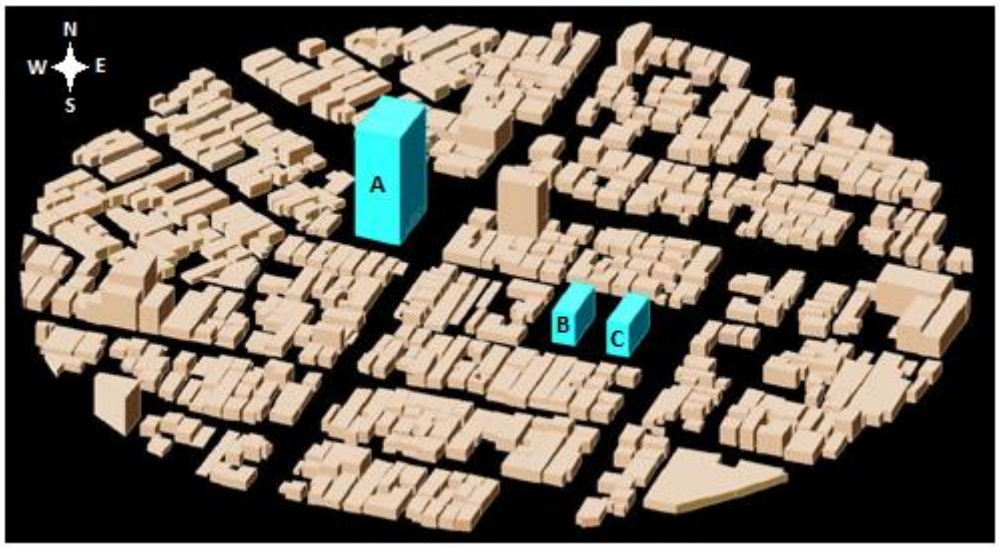

Figure 4.1 Perspective view of geometry of the urban area of Niigata city, Japan (adapted from AIJ [9])

4.1.2 Results

Experimental results from those wind-tunnel measurements for both the wind flow and pollutant concentration field were provided by the AIJ. Concentration is expressed by using the dimensionless concentration coefficient K:

$$K = c\frac{H_{ref}^2\, U_{ref}}{Q_s} \cong 355c \qquad (16)$$

Results are presented in the chapter 2 in Figure 2.10-2.11. Behind the target buildings B and C higher levels of concentration were present. In the source, ethylene (C_2H_4) is being released with a mass fraction, c, of 1, then the maximum concentration 355 was found there. As this maximum is

considerable higher than concentration levels in the other points near the source (39 and 41), measurement point 40, which represents the location where that pollutant was released, was not plotted.

4.2 CFD simulations

Case 2 aims to predict both the wind flow and pollutant concentration field involving an urban area of Niigata city, Japan [9]. This urban area consists of a set of irregular buildings dispersed in the city through an irregular way along its perimeter. Those buildings present a height average of 6 m, but there are buildings from 2 m up to 60 m high. A pollutant source is set near the centre of the urban area. It is being released ethylene (C_2H_4) aiming to assess the pollutant dispersion taking into account west wind direction and by using the RANS equations and the turbulence RNG k-ε model. Wind-tunnel experiments have been conducted by the Architectural Institute of Japan (AIJ) [9] for predicting pollutant dispersion of ethylene. The AIJ provide results of both the wind flow and pollutant concentration field to validate the present research.

4.2.1 Model and computational domain

Based on the scaled model used for the wind-tunnel experiments, the sizing of the computational model at 1:250 scale was arranged using the pre-processor Gambit 2.4.6 to 6.12 m x 3.03 m x 1.20 m as shown in Figure 4.2. The urban area was set inside a drawn circle and divided in eleven sub-domains such as the pieces of a puzzle, in order to mesh them separately before extruding. Thus, the computational requirements, mainly the computational memory required, are not that significant and the domain can be set easier.

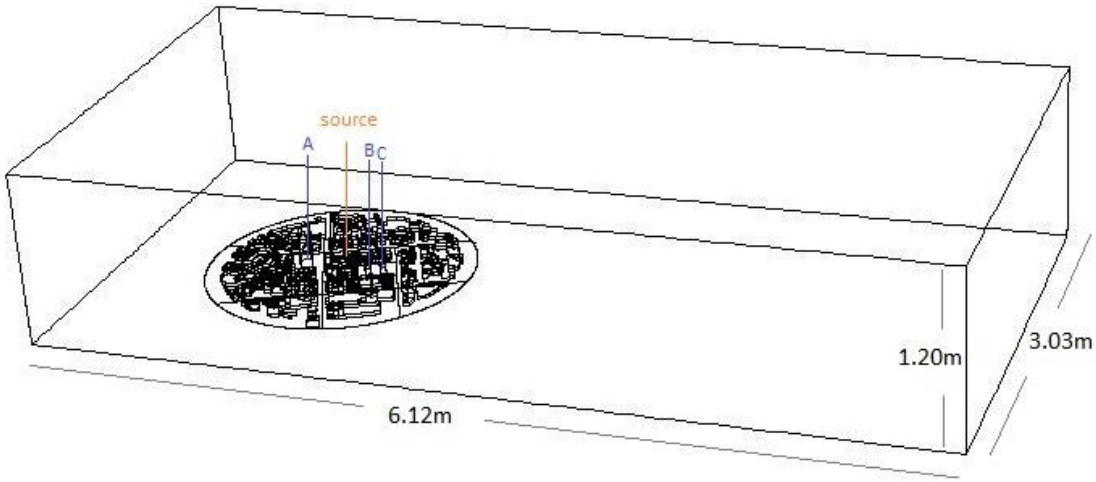

Figure 4.2 Computational domain of the urban area of Niigata city from Case 2

4.2.2 Computational grid

The urban area of Niigata is composed by a set of buildings organized irregularly. The shape of the most part of these buildings is also irregular and their height varies in a wide range between 2 m and 60 m high (full-scale). The first step was the simplification of the shapes in the ground-plane making them more regular. As the density of the buildings in the urban area is high, generating a computational grid with high quality is not guaranteed [14]. Then, taking into account the difference in the heights, the distance between some buildings was deleted and they were connected , sharing the same bound or "wall". This was made when the distance between two buildings was set around 3 m at full-scale (12 mm at reduced-scale) that was consider as a non-significant distance by the user. It can be observed by comparing Figure 4.3 and Figure 4.4. A circle was set around the urban area aiming to

limit it in relation to the rest of the domain. This makes simpler to mesh the space in the surroundings of the urban area.

After this simplification, edges and faces around the buildings' faces were created for meshing the entire ground-plane. In total, the amount of cells at the ground-plane is 429,653 (Figure 4.5). For the domain's height, the number of cells was set to 141 for keeping the stretching ratio 1.3 or less [11,12]. As the total number of cells for the entire domain including the urban area, the finest part, is 60,581,073, meshing the volumes as only one entire domain makes the process hard because the computational memory required. Thus, in order to reduce the computational requirements, ground-plane was divided in eleven smaller areas which generated eleven sub-domains after extrusion. It is shown in Figure 4.4 which buildings were included per each sub-domain. Particularly, the complex 5 is divided in 3 sub-domains (5_I, 5_II and 5_III) and it includes the source that is the finest part of the domain. Figure 4.6 shows the different complexes including the faces of the buildings' surroundings.

Each sub-domain was created by the extrusion of its horizontal ground-plane based on the method that is described by van Hooff and Blocken [14] and that has been used in Case 1. A vertical line was created from one of the vertices (Figure 4.7). This vertical line was divided in edges for the different considered heights of the buildings. Then, the horizontal plane is extruded edge by edge and depending on the height, the internal volumes of those buildings are deleted and the buildings become walls.

Eleven meshes were created and exported to the commercial Fluent 12.1 in which they were connected by using the interfaces previously defined in Gambit 2.4.6. Every single face that is going to be connected against another face has to be set as a specific interface in Gambit before to be exported to Fluent 12.1.

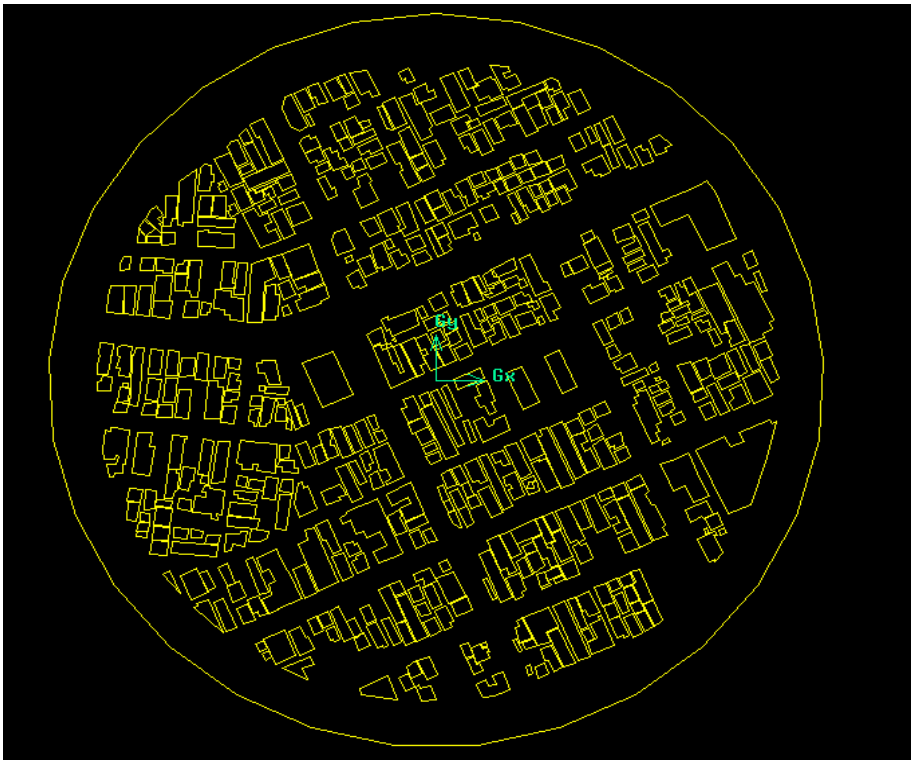

Figure 4.3 Urban area before simplification from Case 2

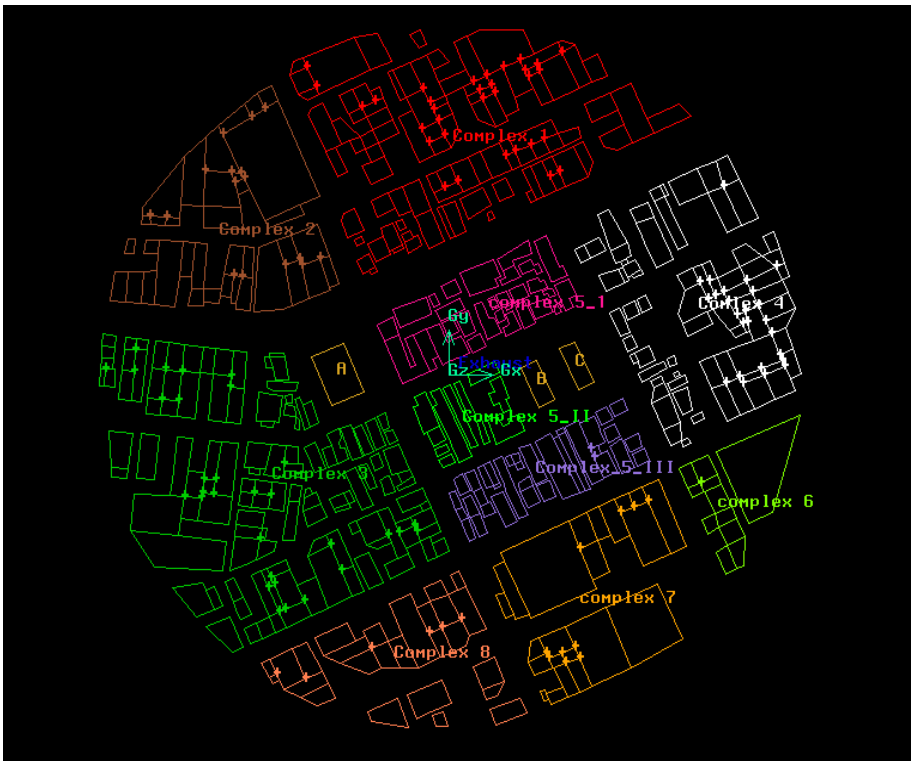

Figure 4.4 Buildings distributed for the eleven sub-domains from Case 2

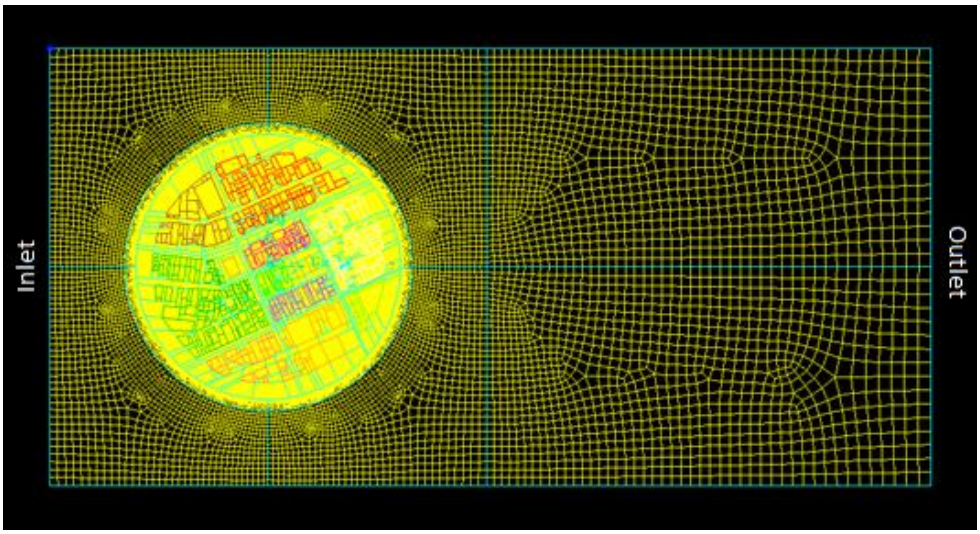

Figure 4.5 Ground-plane meshed before extrusion from Case 2

From Fluent 12.1 it was possible to generate perspective views of the entire domain unified as shown in Figure 4.8. It is possible to observe the target buildings A, B and C. The source is located in the ground-level as indicated by the arrow. With more detail, the target buildings A, B and C are presented through Figure 4.9 and 4.10. The grid arrangement is truly refined near the bottom and the top of the buildings. The urban area is significantly finer than the rest of the domain. The finest sub-domain is the complex 5, mainly near the source once the pollutant C_2H_4 is being released from there. The main aim with Case 2 is to predict the pollutant concentration of that pollutant in the source surroundings which justified the increased number of cells in and near the source as shown in Figure 4.11. Figure 4.11(a) results from a zoom out of Figure 4.11(b).

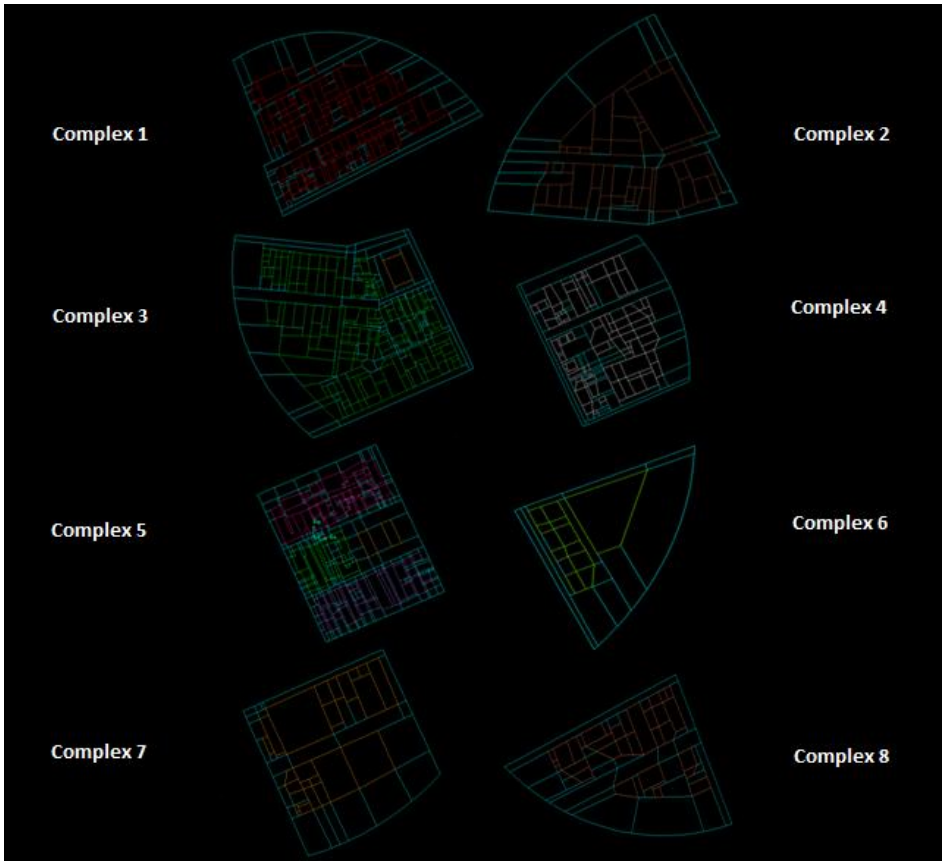

Figure 4.6 Sub-domains called “Complexes” as pieces of a puzzle from Case 2

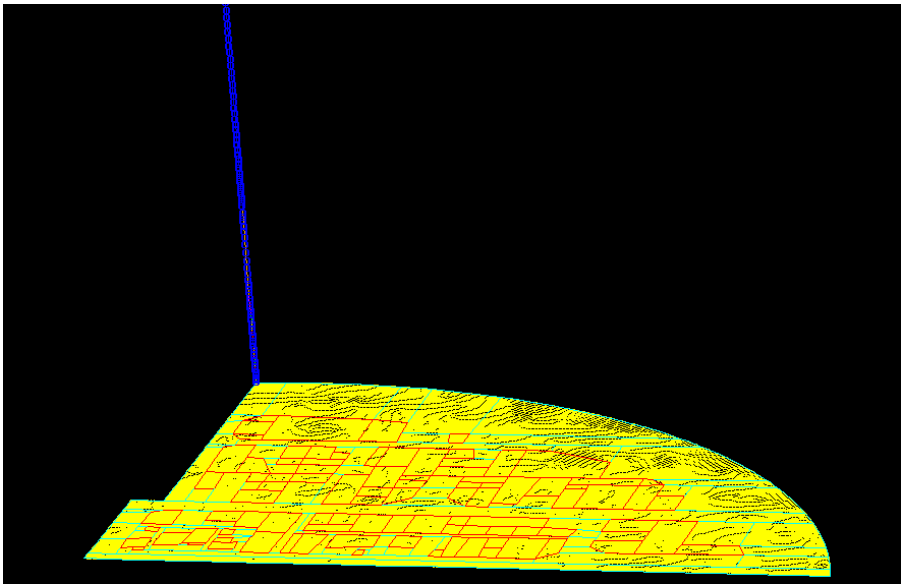

Figure 4.7 Complex 1 ready for extrusion from Case 2

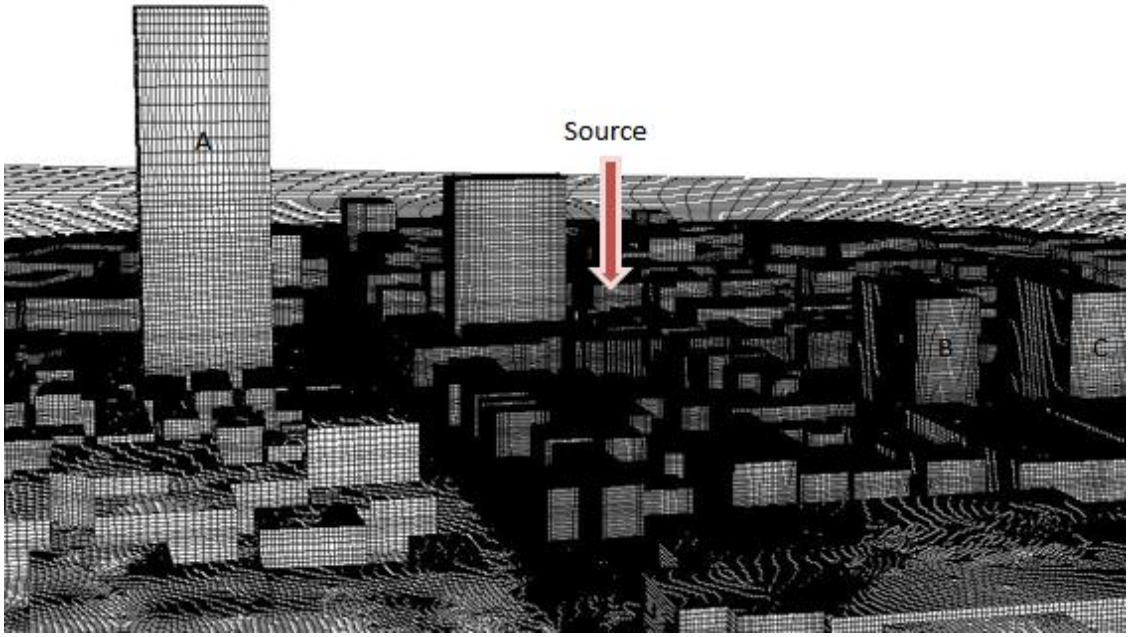

Figure 4.8 Perspective view of the computational grid arrangement from Case 2

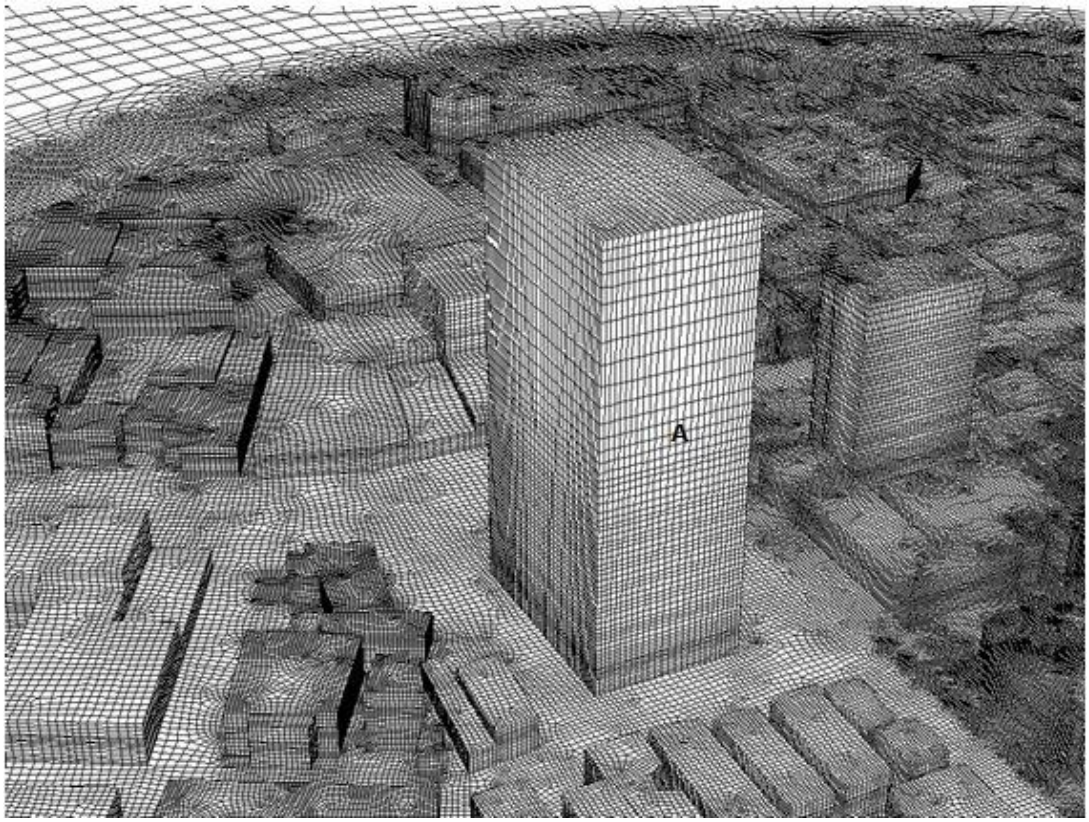

Figure 4.9 Perspective view of target building A from Case 2

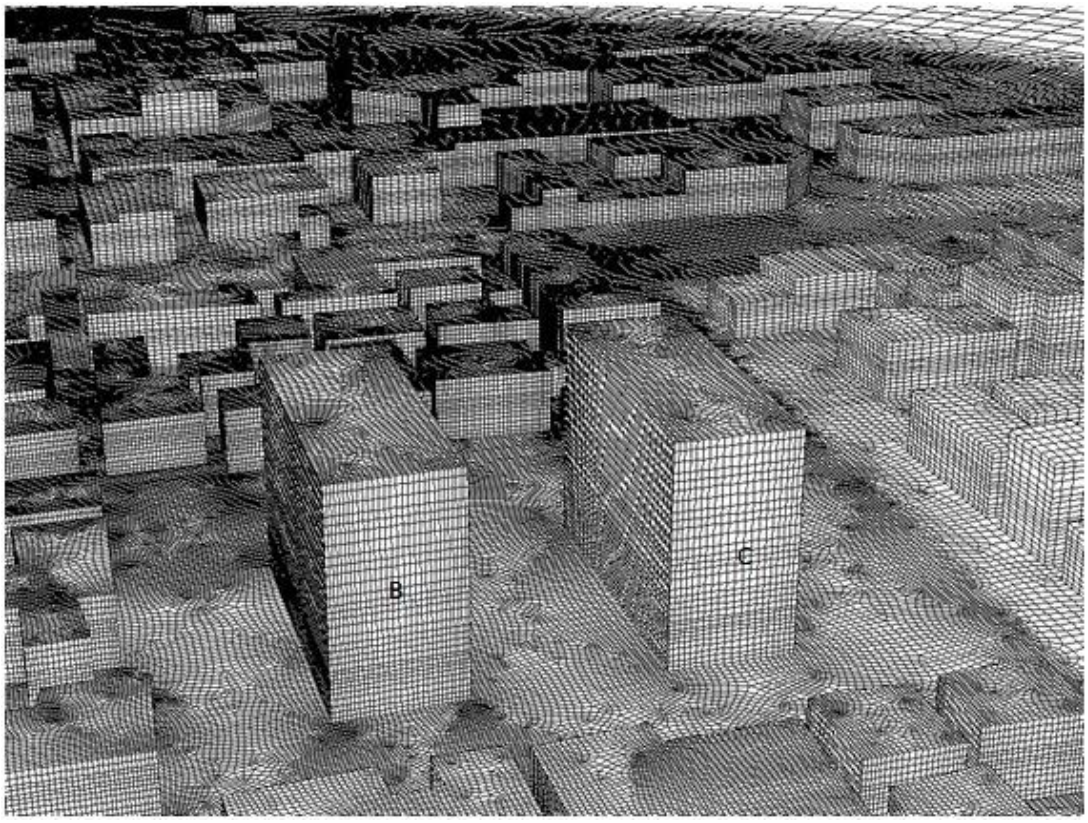

Figure 4.10 Perspective view of both target building B and C from Case 2

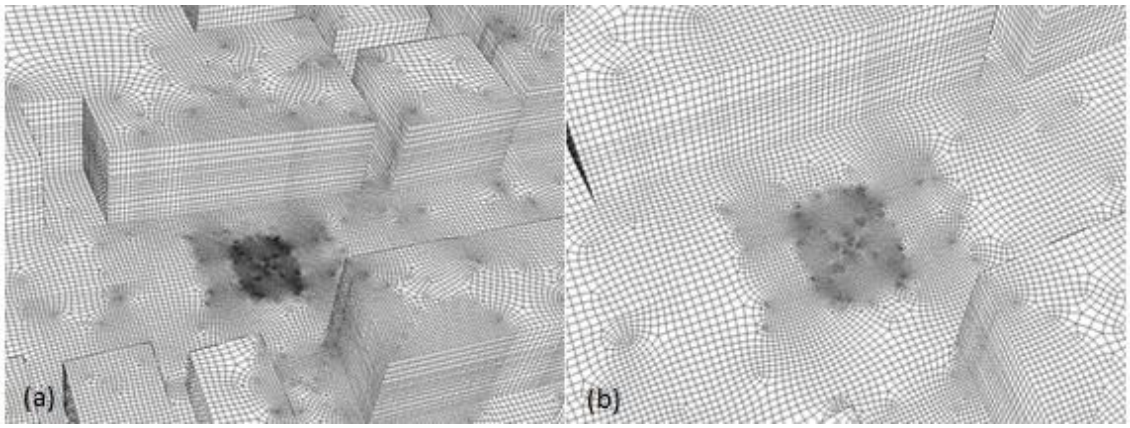

Figure 4.11 (a) Source and (b) Zoom in on the source from Case 2

4.2.3 Boundary conditions

The parameters of the experimental setup were applied to the numerical simulation such as the wind flow and turbulence profiles and the boundary conditions. The boundary conditions are shown in Table 4.1 and some parameters used for calculating them are presented in Table 4.2.

Table 4.1 Boundary conditions from Case 2

Inlet	Velocity inlet
	Momentum: Velocity magnitude U(z)
	Turbulence: k(z), ε(z)
Outlet	Pressure outlet
	Static/Gauge pressure (Pa): 0
	Turbulence: k(z), ε(z)
Bottom	Wall, Shear condition: no slip
	Wall roughness: z_0=0.024, C_s>1 (UDF: C_s=1.4)
Top	Symmetry
Side Walls	Symmetry
Exhaust	z-velocity: 1 m/s
	Turbulence: Intensity and Length scale
	Turbulence intensity: 10%
	Turbulence length scale: 0.00028 m
	Species: ethylene; Mass fraction: 1
Top and side walls of building	Wall
	Shear condition: no-slip
	Wall roughness: k_s=0.0m; C_s=0.5

At the inlet and outlet were used the wind-speed, U(z), and turbulence, k(z) and ε(z), profiles as function of the domain's height, all provided by the AIJ (Table 4.1). Such conditions (Figure 4.12-4.13) have been used in reduced-scale studies of the urban area of Niigata city [8-10].

At the bottom, wall shear condition (no slip) and roughness were both defined. The height of the cells adjacent to the bottom of the domain is approximately 0.362m, which means y_p = 0.181m. Thus, in order to achieve horizontal homogeneity of the wind-speed profile, C_s is calculated based on the statement $k_s<y_p$ and also on the given model surface roughness length z_0 = 0.024m. Applying equation (8), C_s is set to 1.40, considering k_s=0.168. Since the highest possible value of C_s is equal to 1, an UDF has to be used (see Annex II). Top and side walls of the computational domain were defined as symmetry as previously made in Case 1.

The exhaust velocity of the pollutant C_2H_4 is 1m/s, calculated based on momentum (M_s=0.5) and the reference wind-speed on the top of the boundary layer, 2m/s.

Top and side walls of the building were set to default values of shear condition and wall roughness as recommended by Fluent Inc. [13].

Table 4.2 Parameters for calculating boundary conditions

Parameter	Description	Value
α	Power-law exponent	0.250
H_b	Building reference height [m]	0.240
D_s	Source diameter [m]	0.004
W_s	Source velocity [m/s]	1.000
M_s	Source momentum ratio	0.500
A_s	Source surface [m²]	0.0000125
Q_s	Emission rate of the pollutant [m³/s]	0.0000125

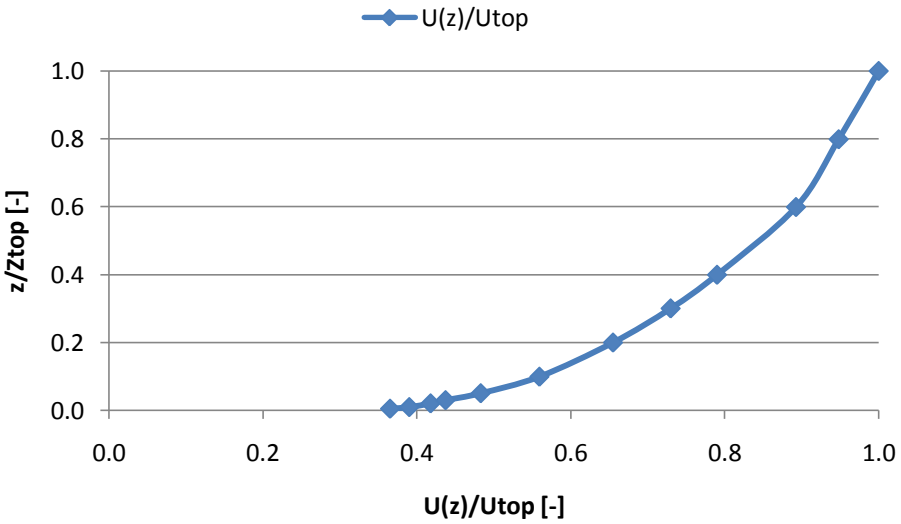

Figure 4.12 Wind-speed profile at the inlet (from the data provided by the AIJ)

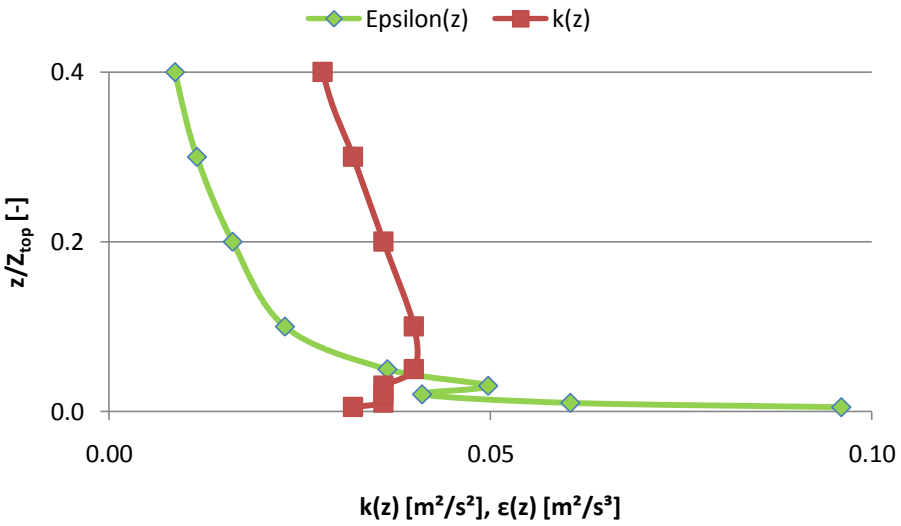

Figure 4.13 Turbulent kinetic energy k profile and turbulence dissipation rate ε profile at the inlet and outlet (from the data provided by the AIJ)

4.2.4 Other computational parameters

Discretization schemes are presented in Table 4.3. The same schemes applied in the previous case (Case 1) were applied with Case 2. The maximum degree of convergence was also set to 10^{-11} for all the variables.

Table 4.3 Discretization schemes in use for calculation

Discretization	Pressure-velocity coupling: SIMPLE (Semi-Implicit Method For Pressure-Linked Equations) Pressure: Second order Momentum, k and ε: Second order upwind Helium, Energy: Second order upwind

4.3 Comparison experiments with simulations

Simulation results will be presented for the wind flow and pollutant concentration field. Wind-peed vectors around the buildings at the pedestrian-level (0.008 m at reduced-scale and 2m at full-scale) are shown in Figure 4.14, through a horizontal view, and in Figure 4.15, through a vertical view. It is possible to observe that behind the target building A wind flow presents the highest wind-speed level (green arrows), and the target buildings B and C are both affected by significant lower wind-speed levels. It is clear recirculation of the wind flow around the source (dark blue).

Figure 4.16 and 4.17 show the same planes of the Figure 4.14-4.15 but through contour levels of the wind-speed. The recirculation behind the buildings is notorious with special attention to the target building A. Figure 4.17 evidences the separation zone of the wind flow also with special attention to the target building A, mainly because its significant height in relation to the other ones. Then, the back region of the building A is characterized by lower wind-speed levels (dark blue) but near of it higher wind-speed levels are achieved.

The horizontal distribution of the pollutant concentration K is shown in Figure 4.18. Recirculation of the wind flow led to pollutant distribution behind the source opposite to the wind direction. In general, the concentration predicted by using RANS is slightly higher than the experimental measurements [9]. Figure 4.19 shows the vertical distribution of the pollutant concentration K which presents higher levels near the target buildings B and C once the wind flow is coming from west.

At the pedestrian-level, near the source, K presents values higher than 50. At the higher heights, ethylene is spread by higher wind-speed levels in the west direction and, consequently, the concentration K becomes significantly lower.

Figure 4.14 Wind-speed vectors (horizontal plane) at the pedestrian-level

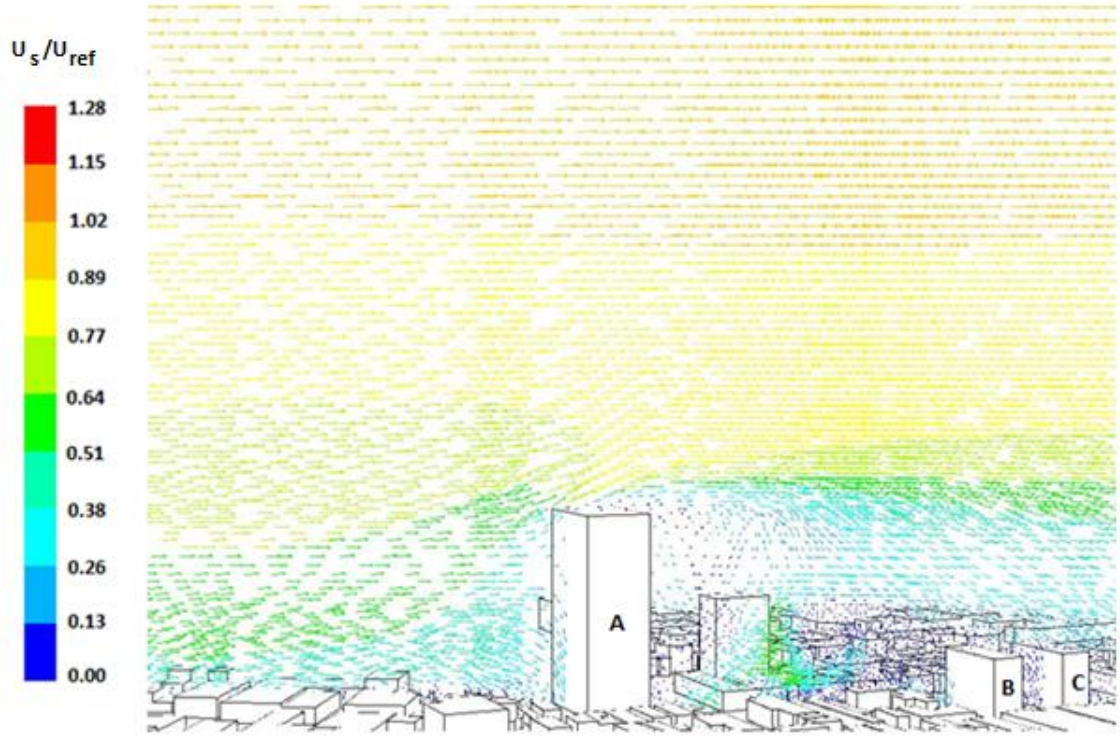

Figure 4.15 Wind-speed vectors (vertical plane, y=0)

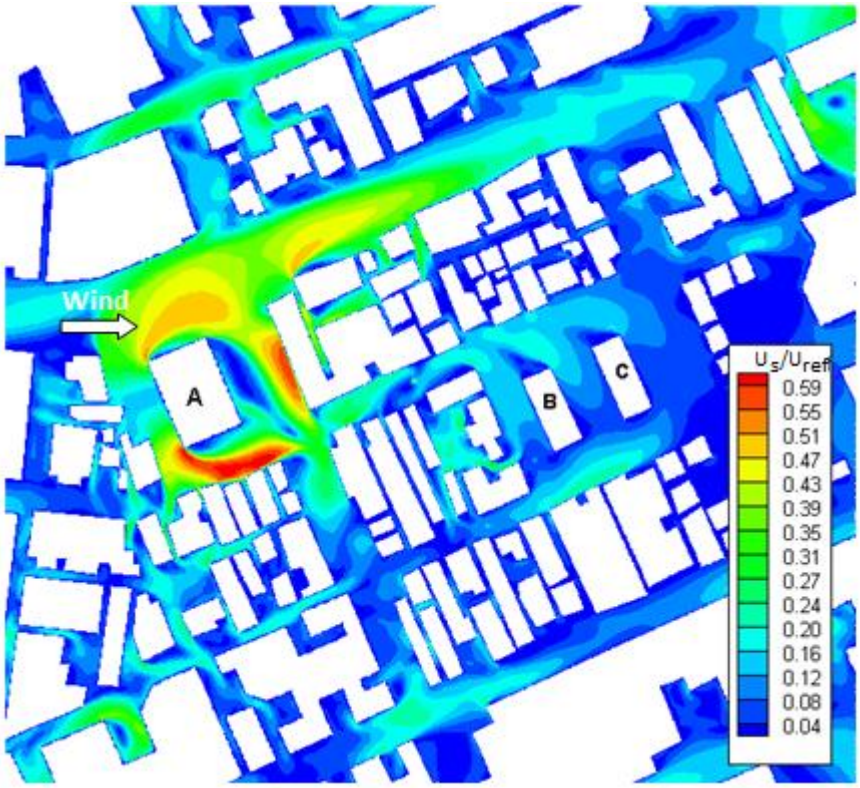

Figure 4.16 Wind-speed contours (horizontal plane) at the pedestrian-level

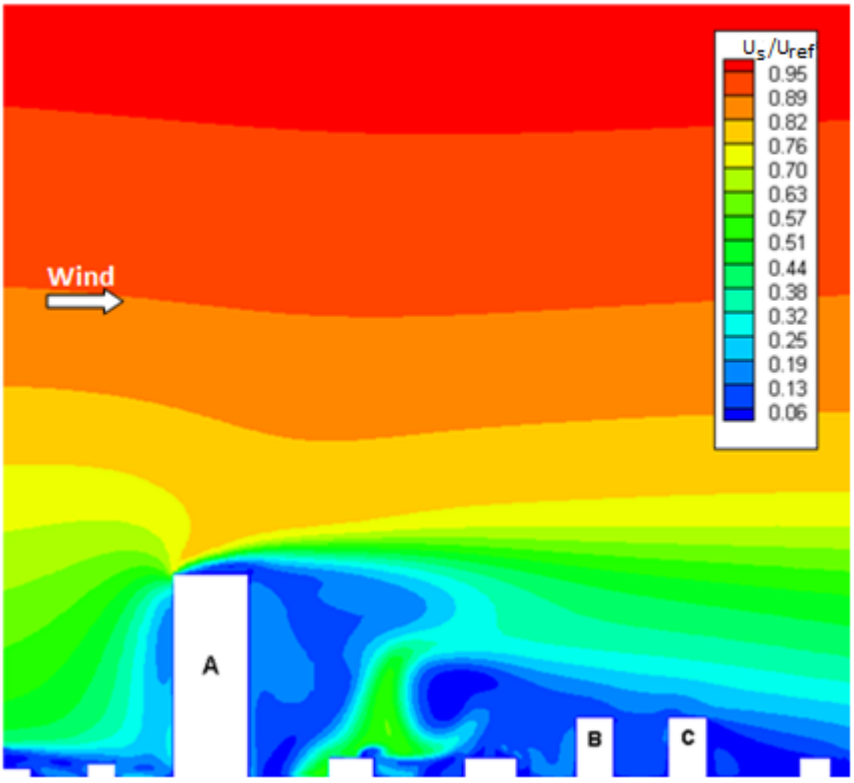

Figure 4.17 Wind-speed contours (vertical plane, y=0)

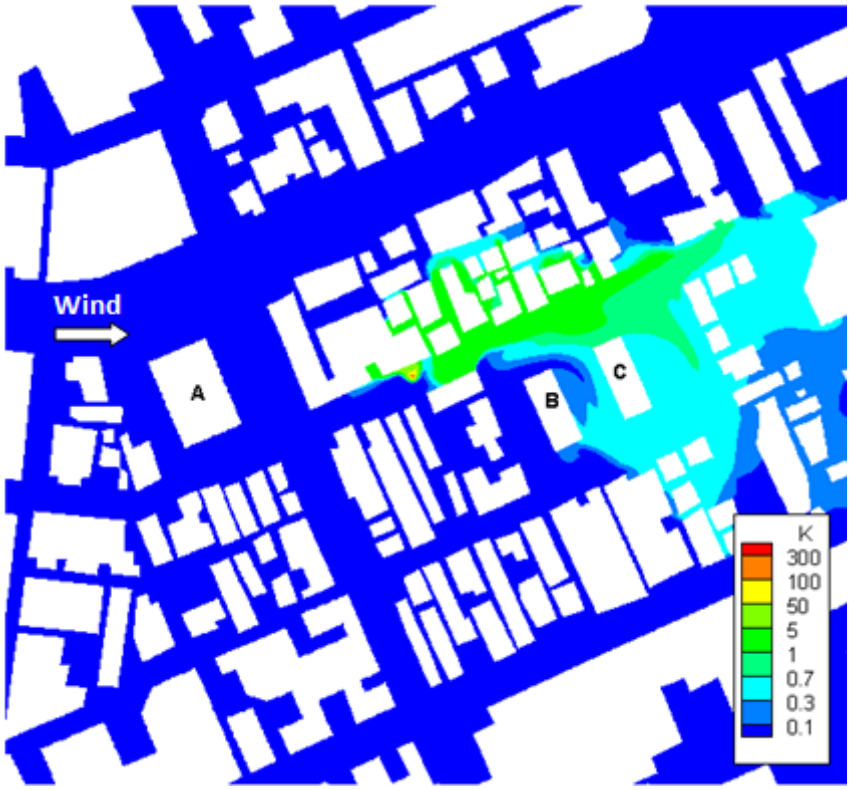

Figure 4.18 Pollutant concentration contours (horizontal plane) at the pedestrian-level

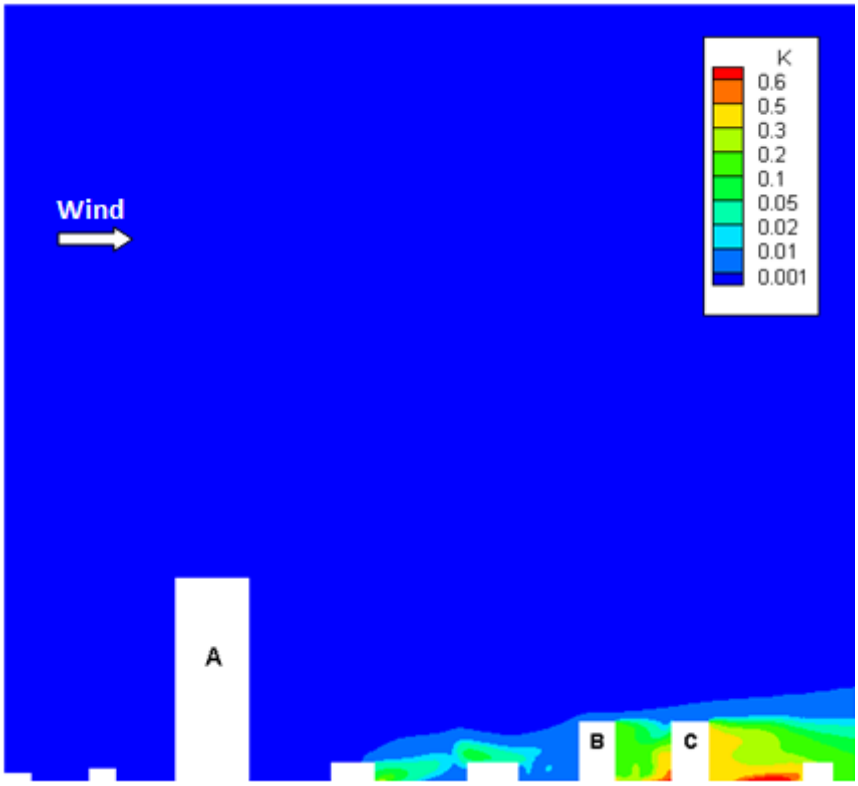

Figure 4.19 Pollutant concentration K contours (vertical plane, y=0)

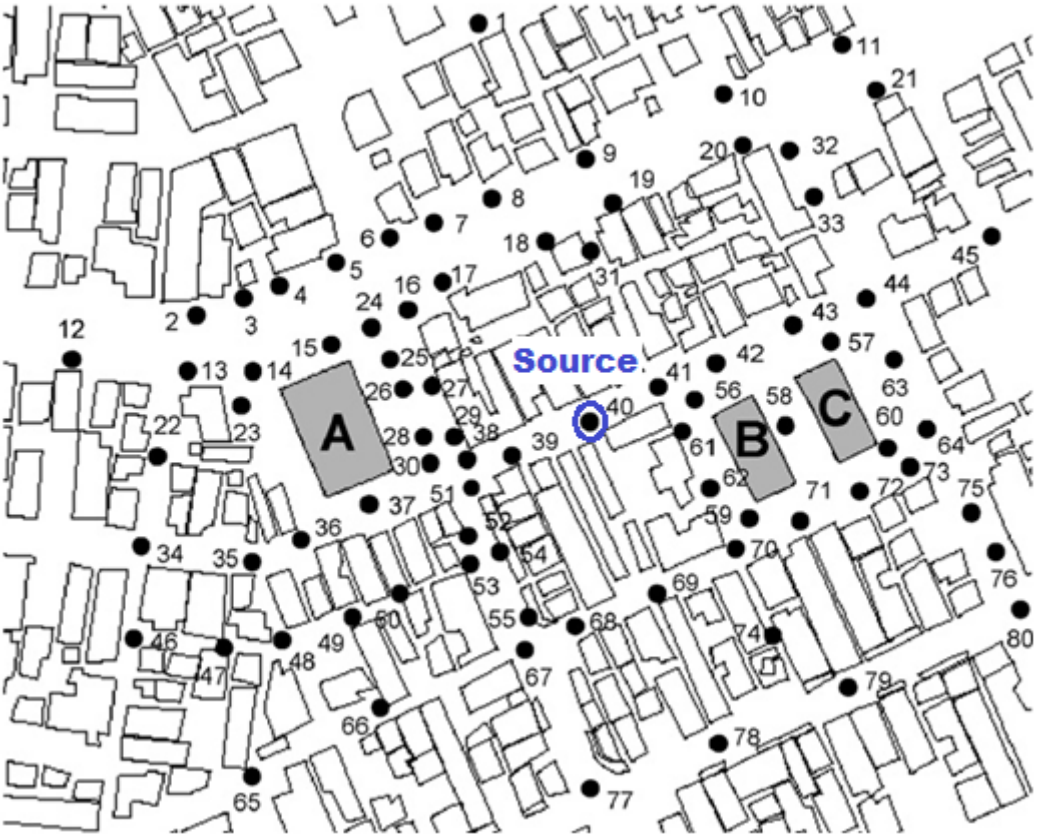

Figure 4.20 Eighty measurement points and source location (provided by the AIJ)

For validating Case 2 with the experimental results (2.10-2.11), both the wind flow and pollutant concentration were quantified in the eighty measurement points considered (see Annex III). Figure 4.20 shows their location. The correlation between CFD results and experimental measurements will be presented in a dimensionless way. As previously discussed for quantifying the agreement of those results, Fractional Bias (FB), Normalized mean square error (NMSE) and Fraction of predictions within a factor of 2 (FAC2) will be calculated as well.

Figure 4.21 compares the wind-speed ratio at each measurement point against the predicted results from Case 2. In general, results from the present case study fairly agree with the experimental ones, mainly, in relation to the points showing high wind-speed ratios. Figure 4.22 compares the pollutant concentration K at each measuring point. The high concentrations at point 32 and 33, are well predicted by RANS. At point 41-43 located near the source, the concentration K is overpredicted by RANS. The same happens behind the target building C, at point 57, 60, 63, 64, 72, 73. In spite of overpredicted in referred locations, the numerical results are logical.

The correlation by comparing both numerical and experimental results is shown in Figure 4.23-4.24. The computed results underpredicted the wind-speed ratios behind the buildings in general. This can evidence difficulties of the RANS in predicting the wind flow accurately in that kind of regions.

Table 4.4 lists the statistical factors to quantify the agreement between the results for the wind-speed ratio. All those factors presented logic results by following the wind-speed and pollutant concentration patterns from the experiments [9]. As a result of the overprediction of the concentration K in some locations, the correlation between the numerical and experimental results presents large variations because at some points that concentration is overpredicted. Table 4.5 shows that NMSE represents the worst quantification of agreement that can be explained by such overprediction behind the target building C.

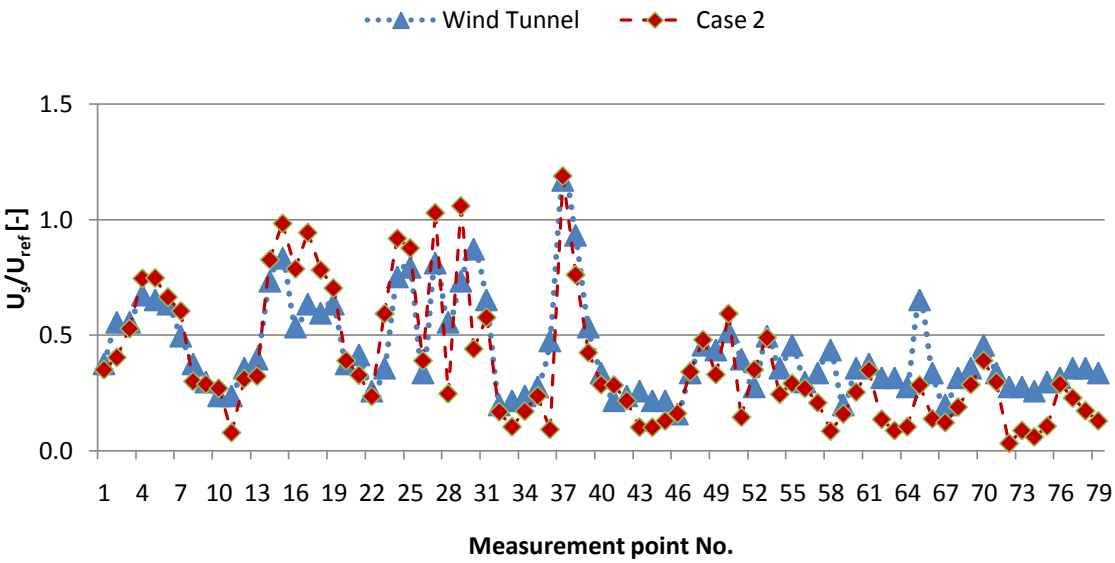

Figure 4.21 Comparison of wind-speed ratios at each measurement point

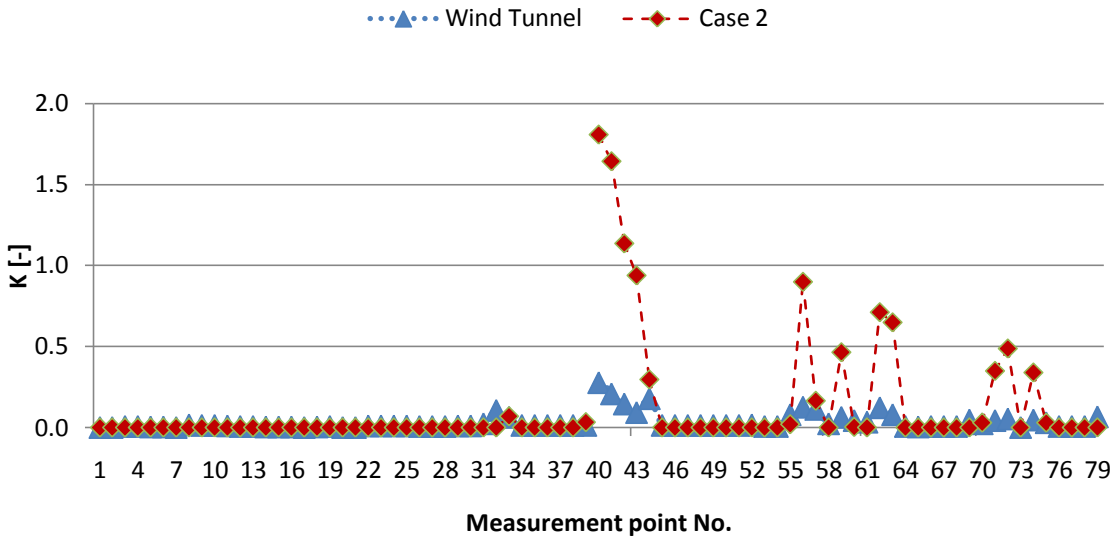

Figure 4.22 Comparison of pollutant concentration K at each measurement point

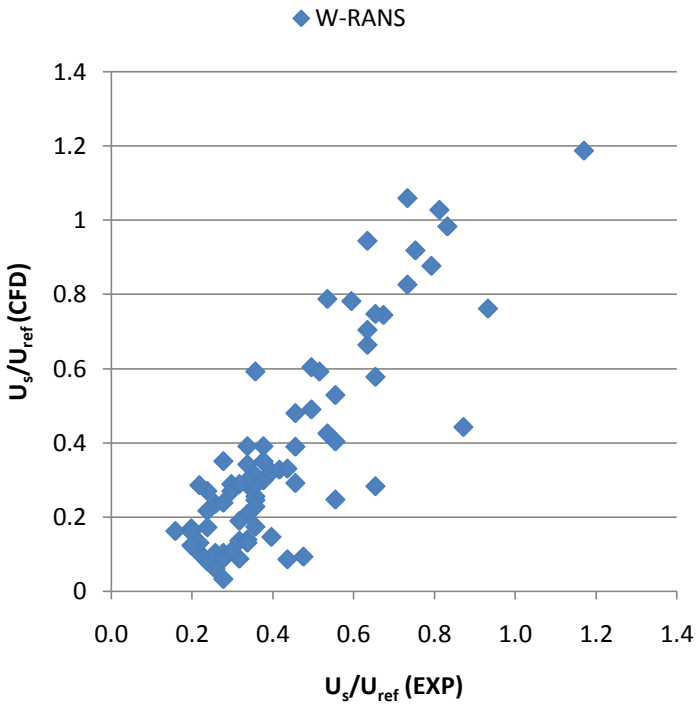

Figure 4.23 Correlation between numerical (CFD)and experimental (EXP) wind-speed ratio

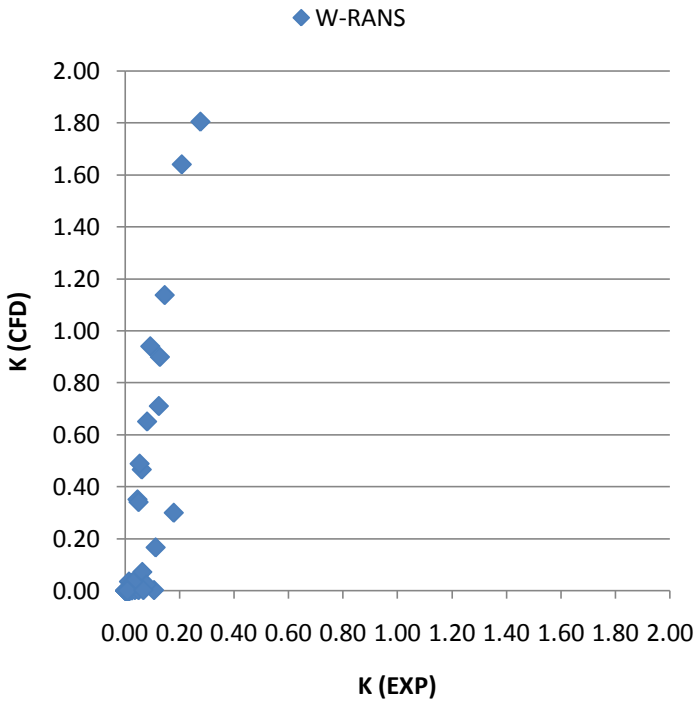

Figure 4.24 Correlation between numerical (CFD) and experimental (EXP) of pollutant concentration K

Table 4.4 Statistical factors for wind-speed ratio

U_s/U_{ref}	FB	NMSE	FAC2
W-RANS	0.134	0.154	0.759

Table 4.5 Statistical factors for dimensionless concentration K

K	FB	NMSE	FAC2
W-RANS	-1.181	23.894	0.063

4.4 Discussion and conclusions

It was predicted the wind flow and pollutant concentration field of ethylene released from near the centre of the urban area. For both cases, the validation is made by comparing against the wind-tunnel measurements performed and provided by the Architectural Institute of Japan (AIJ).

The wind flow field predicted presents fair agreement with the wind-tunnel measurements in the different locations as shown by Figure 4.23 which is expressed by the correlation between the CFD and experimental results and through the statistical factors. FB and NMSE should be zero in a perfect scenario in which CFD results are equal to experimental measurements. FAC2 should be one. Observing those results expressed in the Table 4.4, the agreement is fair.

Validation of the pollutant concentration field followed the same methodology of the wind flow field. The pollutant concentration K were predicted for the eighty different locations set in the urban area at the pedestrian-level (0.008 m at reduced-scale and 2 m at full-scale). After comparing against the wind-tunnel measurements, it was observed acceptable agreement with some exceptions. Near the source and behind the target buildings B and C overprediction was verified at some point locations. Those overpredictions might be explained by the difficulties in predicting the wind flow behind a building using the turbulence model approach RANS.

In general, concentration results show fair agreement by comparing against the wind-tunnel measurements because they follow the same patterns. However, the correlation between the CFD and experimental results and the statistical factors are negatively influenced by those overpredicted points. By observing those validation metrics the worst one is the NMSE. In the other hand, FB and FAC2 show more acceptable results.

5. Discussion

Two simulations were performed in Case 1 using two different grids, one coarser and another one finer. It was concluded that there were not significant variations on the prediction of pollutant dispersion. This grid sensitivity analysis made possible to use the coarser grid which requires less computational resources and consequently less time-consuming. These simulations were performed using the same boundary conditions and turbulence model approach RANS through RNG k-ε model. In fact, results present underprediction in relation to the wind-tunnel and numerical experiments performed by Li and Meroney [7] and Gousseau et al. [6], respectively. In spite of that, it is clear recirculation on the rooftop as in the wind-tunnel and numerical experiments referred. After the sensitivity analysis, two more turbulence models were used: Realizable k-ε model and RSM. The results were not improved in relation to the simulation performed by using the RNG k-ε model. Actually, Realizable k-ε model was not able to reproduce recirculation on the rooftop. In conclusion, the RNG k-ε model and RSM, which both can reproduce recirculation on the rooftop, presented the closest results in relation to the wind-tunnel and numerical experiments. This had been concluded by Gousseau et al. [6] as well.

In order to understand which factor could be the reason of the underpredicted results, it was tested what is the influence of the turbulent kinetic energy profile k. That profile was calculated based on the turbulence intensity I_u from Li and Meroney [7]. Then, more simulations were performed using different k profiles: 0.25k, 0.5k and 2k. 0.25k profile has shown better agreement with the wind-tunnel [7] and numerical [6] results for the recirculation levels on the rooftop. This evidences turbulence kinetic energy k truly influences the recirculation level on the rooftop and consequently the dispersion of the pollutants released from the vent showing there can be some incoherencies between the k profile used in Case 1 and that one used by Gousseau et al. [6] once it is unknown which turbulent kinetic energy k profile has been used by [6].

The model of the urban area of Niigata city (Case 2) requires huge computational resources because of the very large grid arrangement. Consequently, it is very time-consuming to simulate the wind flow and pollutant concentration field. It was predicted the wind flow and pollutant concentration field of a pollutant (ethylene) being released near the centre of the urban area. Studies have been conducted by the Architectural Institute of Japan (AIJ) [9] in order to predict the wind flow field in the urban area of Niigata city [8]. These studies include wind-tunnel measurements with a reduced-scale model. In chapter 4, the validation of the wind flow and pollutant concentration field caused by that pollutant was presented. For both cases, the validation is made by comparing against those wind-tunnel measurements performed and provided by the AIJ.

The wind flow field predicted presents fair agreement with the wind-tunnel measurements in the different locations as shown by the Figure 4.23 which is expressed by the correlation between the numerical and experimental results and through statistical factors. FB and NMSE should be zero in a perfect scenario in which numerical results are equal to the experimental measurements. FAC2 should be one. Observing Table 4.4, the agreement is fair.

Validation of the pollutant concentration followed the same methodology as it has been made to the wind flow field. The values of pollutant concentration K were predicted for the eighty different locations set in the urban area at the pedestrian-level (0.008 m at reduced-scale and 2 m at full-scale). After comparing against the wind-tunnel measurements, it was observed acceptable agreement with some exceptions. Near the source and behind the target buildings B and C overprediction was verified at some point locations. These overpredictions might be explained by the difficulties in predicting the wind flow behind buildings by using the turbulence model approach RANS. However, results show fair agreement by comparing against the wind-tunnel measurements because predictions follow the same patterns. The correlation between the numerical and experimental measurements and the statistical factors are negatively influenced by those overpredicted points. The worst one is the NMSE. In the other hand, FB and FAC2 show more acceptable results.

The overprediction at some point locations of the urban area can be influenced by the source location. A deviation in the precise location comparing against the wind-tunnel model can be enough

to change the results. Blocks of buildings are really close to the source and their influence on the pollutant dispersion can be significant as well.

For both Case 1 and Case 2, there are some incoherencies between the predicted and measured concentration K which influence the results validation. Such incoherencies can be related with limitations of the turbulence models and approach, discretization parameters or boundary conditions. Sensibility analysis of those incoherencies can lead to better predictions. The turbulent kinetic energy k sensibility has been tested in Case 1. In fact results reported significant modifications on the recirculation on the rooftop of the building by decreasing such profile. Concentration levels were not significantly better predicted but recirculation levels were improved. Sensibility analysis were not provided in Case 2 because the time required for simulating.

6. Conclusion and final recommendations

Through CFD is possible to test easily variations on boundary conditions and discretization. Also building modifications can be made introducing or removing new buildings, varying their position or adding pollutant sources. Two different cases with an increasing level of complexity have been presented aiming to assess the accuracy of CFD in predicting the pollutant concentration distributions around buildings.

Firstly, a simple model of an isolated cubic building (chapter 3) was set based on the wind-tunnel experiments [7] and the predictions conducted by Gousseau et al. [6]. Both experimental and numerical models referred have been used for validation. Then, it was predicted the pollutant dispersion around an isolated cubic building. Three simulations were performed by using turbulence model approach RANS through the turbulence models RNG k-ε model, Realizable k-ε model and RSM. In general, pollutant concentration is underpredicted on the rooftop and behind the isolated cubic building. Separation of the fluid flow and recirculation on rooftop are reproduced with fair agreement for both RNG k-ε model and RSM.

Secondly, from a model of an urban area of Niigata city, Japan, the Architectural Institute of Japan (AIJ) [9] has performed wind-tunnel measurements for both the wind flow and pollutant concentration field (chapter 4). Its level of complexity is significantly higher than the previous isolated cubic model because it treats a model composed by many irregular buildings irregularly distributed. Thus, it is not guaranteed to arrange a grid with enough quality. More computational resources are required which results in more time consumed for arranging that grid and then performing simulations. Turbulence was modeled by using RANS approach through the turbulence model RNG k-ε model. Results show fair agreement for both the wind flow and pollutant concentration field. However, concentration field, quantified by the pollutant concentration coefficient K, is overpredicted at some predicted points (see Annex III), mainly near the source and behind the target building C. This leads to poor correlation between numerical and experimental results.

The grid arranged for the urban area of Niigata city has a total number of cells around 60 millions. Because of the time-consuming required to make a grid-sensitivity analysis, that was not provided. In the future, it would be an useful step for both assessing the discretization errors and to decrease the time of the simulation. It would be recommended to perform simulations by using LES as well. In general, for predicting pollutant dispersion, LES has shown better agreement with the full-scale and wind-tunnel experiments than RANS [24]. With RANS the turbulence is an approximation made by the turbulence model applied such as the k-ε models or RSM. Also more wind directions could be tested and validated by measurements from the AIJ.

7. References

[1] Blocken, B., Stathopoulos, T., Carmeliet, J., Hensen, Jan L.M., 2011, Application of computational fluid dynamics in building performance simulation for the outdoor environment: an overview', Journal of Building Performance Simulation, 4: 2, 157 — 184, First published on: 21 October 2010 (iFirst)

[2] Peterka, J.A., Meroney, R.N. and Kothari, K.M., 1985, Wind flow patterns about buildings. Journal of Wind Engineering and Industrial Aerodynamics 21, p. 21-38

[3] Huijbregts, Z., 2010, Master thesis "Numerical assessment of pollutant concentration distribution around buildings", 2010, Building Physics and Systems, Faculty of Architecture, Building and Planning, Eindhoven University of Technology

[4] Hosker, R.P., 1979, Empirical estimation of wake cavity size behind block-type structures. Preprints of Fourth Symposium on Turbulence, Diffusion, and Air Pollution, Reno, Nev., Jan. 15-18. American Meteorological Society, Boston, Massachusetts. p. 603-609

[5] Blocken B., 2014, 50 years of Computational Wind Engineering: Past, present and future. Journal of Wind Engineering and Industrial Aerodynamics 129: 69-102

[6] Gousseau P., Blocken B., van Heijst G.J.F., 2011,CFD simulation of pollutant dispersion around isolated buildings: On the role of convective and turbulent mass fluxes in the prediction accuracy. Journal of Hazardous Materials 194, 2011, 422-434

[7] Li, W. and Meroney, R., 1983, Gas dispersion near a cubical model building. Part I. Mean concentration measurements, Fluid Mechanics and Wind Engineering Program, Department of Civil Engineering Colorado State University, Fort Collins, CO 80523 (U.S.A.)

[8] Tominaga, Y., Yoshie, R., Mochida, A., Kataoka, H., Harimoto, K., Nozu, T., 2005, Cross Comparisons of CFD Prediction for Wind Environment at Pedestrian-level around Buildings. Comparison of Results for Flow field around Building Complex in Actual Urban Area, The Sixth Asia-Pacific Conference on Wind Engineering (APCWE-VI) Seoul, Korea, September 12-14, 2005

[9] http://www.aij.or.jp/jpn/publish/cfdguide/index_e.htm (October 2014)

[10] Yoshie, R., Mochida, A., Tominaga Y., Kataoka, H., Harimoto, K., Nozu, T., Shirasawa, T., 2007, Cooperative Project for CFD predicition of pedestrian wind environment in the Architectural Institute of Japan. Volume 95, Issues 9-11, October 2007, Pages 1551-1578

[11] Franke, J., Hellsten, A., Schlünzen, H., Carissimo, B., 2007, Best practice guideline for the CFD simulation of flows in the urban environment, COST Action 732, 2007

[12] Tominaga, Y., Mochida, A., Yoshie, R., Kataoka, H., Nozu, T., Yoshikawa, M., Shirasawa, T., 2008, AIJ guidelines for practical applications of CFD to pedestrian wind environment around buildings, JWEIA 96, 2008, 1749–1761

[13] Fluent 6.3 User's Guide, 2006. Fluent Inc., Lebanon

[14] van Hooff T., Blocken B., 2010, Coupled urban wind flow and indoor natural ventilation modelling on a high-resolution grid: a case study for the Amsterdam ArenA stadium, Environmental Modelling & Software 25(1): 51-65

[15] Richards, P.J., Hoxey, R.P., 1993, Appropriate boundary conditions for computational wind engineering models using the k-ε turbulence model. Journal of Wind Engineering and Industrial Aerodynamics 46&47 145-153

[16] Blocken, B., Carmeliet, J., and Stathopoulos, T., 2007, CFD evaluation of wind-speed conditions in passages between parallel buildings – effect of wall-function roughness modifications for the atmospheric boundary layer flow, JWEIA 95 (9–11), 941–962

[17] Wang, X., 2006, Numerical simulation of wind-induced dispersion of emissions from rooftop stacks, M.A.Sc thesis, Department of Building, Civil and Environmental Engineering, Concordia University, Montreal, Canada

[18] Tominaga, Y. and Stathopoulos, T., 2007, Numerical simulation of dispersion around an isolated cubic building – influence of turbulence models and turbulent Schmidt number, Proceedings of 12th international conference on wind engineering, Cairns, Australia

[19] Blocken B., Stathopoulos T., Saathoff P., Wang X., 2008, Numerical evaluation of pollutant dispersion in the built environment: comparisons between models and experiments. Journal of Wind Engineering and Industrial Aerodynamics 96(10-11): 1817-1831

[20] Tominaga, Y. and Stathopoulos, T., 2008, Numerical simulation of plume dispersion around an isolated cubic buildings: comparisons between RANS and LES computations, BBAA VI International Colloquium on Bluff Bodies Aerodynamics and Applications, 20–24 July 2008, Milano, Italy

[21] Stathopoulos, T., Lazure, L., Saathoff, P., Gupta, A., 2004, The Effect of Stack Height, Stack Location and Rooftop Structures on Air Intake Contamination: A Laboratory and Full-scale Study. Montreal, Canada

[22] Gousseau, P., Blocken, B., Stathopoulos, T., van Heijst, G.J.F., 2011, CFD simulation of near-field pollutant dispersion on a high-resolution grid: a case study by LES and RANS for a building group in downtown Montreal. Atmospheric Environment 45(2),428–438

[23] Heist,D., et al., 2013, Estimating near-road pollutant dispersion: a model inter-comparison, Transportation Research, Part D: Transport and Environment., Volume 25, 93-105, December 2013

[24] Tominaga, Y., Stathopoulos, T., 2013, CFD simulation of near-field pollutant dispersion in the urban area environment: A review of current modeling techniques

Annex

I. From Case 1, turbulence dissipation rate ε and roughness constant C_s profile

```
/* BOUNDARY PROFILES FOR WIND-SPEED        Uref = 4.5 m/s */
/* ROUGHESS LENGTH                                  yo = 0.3 m */

real v = 3.3;
real uf = 0.22;
real yo = 0.000075;

/* CALCULATION OF THE PROFILE FOR TURBULENCE DISSIPATION RATE */

DEFINE_PROFILE(eps, thread, nv) /* function name, thread and variable number */
{
      face_t f;
      real x[ND_ND];
      begin_f_loop (f,thread)
      {
      F_CENTROID(x,f,thread);
      F_PROFILE(f,thread,nv) = (uf*uf*uf)/(0.42*(yo+x[1]));
      }
      end_f_loop(f,thread)
}

DEFINE_PROFILE(Cs,t,i)
{
      face_t f;
      begin_f_loop(f,t)
      {
      F_PROFILE(f,t,i) = 3.7;
      }
      end_f_loop(f,t)
      }
```

II. From Case 2, roughness constant C_s profile

```
/* BOUNDARY PROFILES FOR WIND-SPEED        Uref = 2 m/s */
/* ROUGHESS LENGTH                                  yo = 0.024 m */

real v = 1.09;
real uf = 1;
real yo = 0.024;

DEFINE_PROFILE(Cs,t,i)
{
      face_t f;
      begin_f_loop(f,t)
      {
      F_PROFILE(f,t,i) = 1.4;
      }
      end_f_loop(f,t)

      }
```

III. From Case 2, both experimental (EXP) and predicted (CFD) pollutant concentration for 100K

Annex III.a Measurement points 1-40 and percentage of error

Point No.	100K (EXP)	RNG k-ε model		Point No.	100K (EXP)	RNG k-ε model	
		100K (CFD)	%error			100K (CFD)	%error
1	0.01	0.00	100.0	21	0.16	0.00	99.4
2	0.09	0.00	100.0	22	1.28	0.00	100.0
3	0.83	0.00	100.0	23	1.20	0.00	100.0
4	0.70	0.00	100.0	24	1.07	0.00	100.0
5	0.55	0.00	100.0	25	1.04	0.00	100.0
6	0.32	0.00	100.0	26	0.92	0.00	99.9
7	0.10	0.00	100.0	27	0.86	0.00	100.0
8	1.78	0.00	100.0	28	0.85	0.00	100.0
9	1.47	0.00	100.0	29	0.98	0.00	100.0
10	1.37	0.00	100.0	30	0.96	0.00	100.0
11	1.12	0.00	100.0	31	2.48	0.00	100.0
12	0.63	0.00	100.0	32	10.61	0.08	99.2
13	0.67	0.00	100.0	33	6.28	7.04	12.2
14	0.51	0.00	100.0	34	1.36	0.00	100.0
15	0.46	0.00	100.0	35	1.61	0.00	100.0
16	0.37	0.00	100.0	36	1.47	0.00	100.0
17	0.11	0.00	100.0	37	1.44	0.00	100.0
18	0.62	0.00	100.0	38	1.34	0.11	91.6
19	0.65	0.00	100.0	39	1.38	3.40	145.3
20	0.23	0.00	98.7	40	35500.00	638.04	98.2

Annex III.b Measurement points 41-80 and percentage of error

Point No.	100K (EXP)	RNG k-ε model		Point No.	100K (EXP)	RNG k-ε model	
		100K (CFD)	%error			100K (CFD)	%error
41	27.67	180.63	552.8	61	4.41	0.44	89.9
42	20.78	164.18	690.2	62	3.51	0.13	96.3
43	14.56	113.73	681.2	63	12.34	71.12	476.4
44	9.38	94.00	902.5	64	8.03	65.02	710.1
45	17.92	29.86	66.7	65	0.67	0.00	100.0
46	1.44	0.00	100.0	66	0.54	0.00	100.0
47	1.33	0.00	100.0	67	0.76	0.00	100.0
48	1.39	0.00	100.0	68	0.83	0.00	100.0
49	1.36	0.00	100.0	69	0.83	0.01	98.4
50	1.29	0.00	100.0	70	4.89	0.10	98.0
51	1.39	0.00	99.7	71	2.57	2.99	16.4
52	1.35	0.01	99.0	72	4.49	35.00	680.3
53	1.65	0.00	100.0	73	5.38	48.90	809.7
54	0.87	0.00	99.8	74	0.24	0.08	67.3
55	0.69	0.00	100.0	75	4.88	33.97	596.5
56	7.96	2.18	72.7	76	2.94	3.24	10.1
57	12.72	89.92	607.0	77	0.83	0.00	100.0
58	11.33	16.59	46.4	78	0.89	0.00	100.0
59	2.30	0.08	96.5	79	0.78	0.01	98.8
60	6.23	46.56	647.7	80	6.77	0.03	99.6